A Primer on Neural Signal Processing

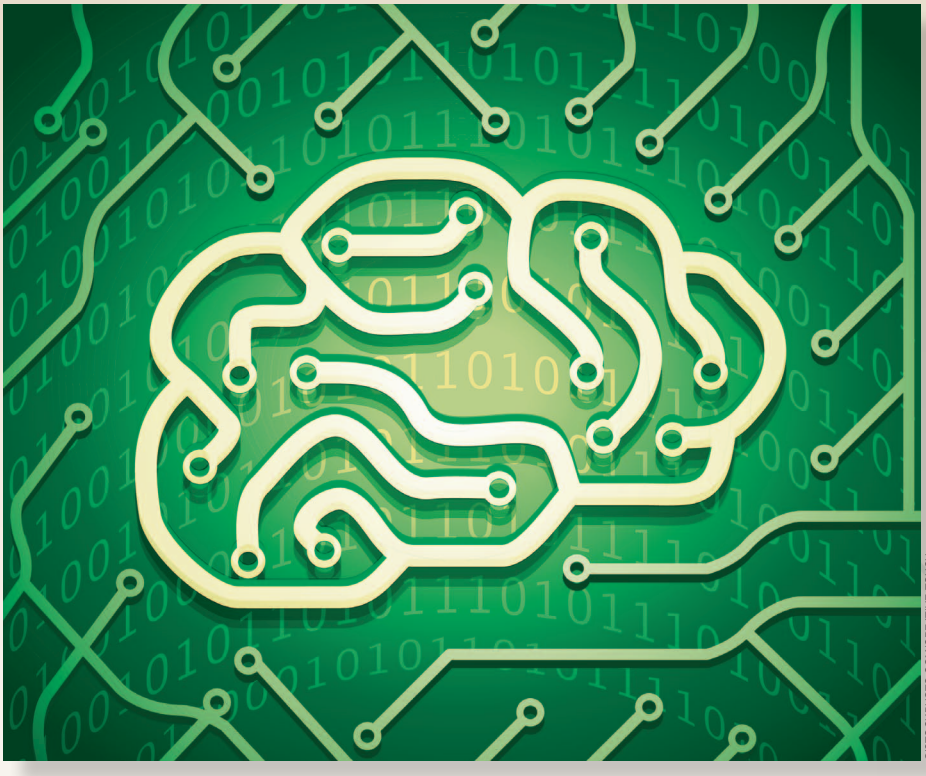

Zhe Chen

Abstract

The role of neural signal processing has become increasingly important in the field of neuroscience with the increase of complexity and scale in neural recordings. In neuroscience, neural signal processing is aimed to extract information from neural signals for the purpose of understanding how the brain represents and transmits information through neuronal ensembles. In neural engineering, neural signal processing is aimed to read out neural signals to send neurofeedback to the brain or computer devices that assist or facilitate brain-machine communications. Here we provide a short review of neural signal processing on important principles and state-of-the-art research. Through representative examples, we illustrate how statistical signal processing can be applied to many diverse neuroscience applications.

Digital Object Identifier 10.1109/MCAS.2016.2642718
Date of publication: 13 February 2017

I. Introduction

Signal processing is a discipline that encompasses the fundamental theory, applications, algorithms, and implementations of processing or transferring information contained in signals. Over the past decades, many statistical signal processing tools have been developed for neuroscience data [1]. Roughly speaking, we can classify fundamental tasks of statistical signal processing into three categories: *signal recovery* (which includes a wide range of inverse problems such as filtering, detection, denoising, deconvolution), *representation and visualization* (e.g., spectral analysis, subspace identification, compression), and *prediction and control*. Rooted in stochastic processes and statistical principles, neural signal processing (**BOX 1**) combines many methods for neural data analysis, among which statistical modeling and

BOX 1: Neural signal processing

Neural signal processing is an emerging discipline that combines statistical signal processing, statistics, control and optimization methods to process neural or neuronal data of diverse sources. Unlike traditional signal processing assumptions, neural signal processing often deals with neurophysiological signals with non-Gaussianity, non-stationarity and heterogeneity.

inference play an important role. Specifically, likelihood and Bayesian approaches are two fundamental inference principles [2]–[5]. In practice, we need to adapt our optimal strategy according to the question of interest.

In this paper, we present a tutorial on neural signal processing for the reader of *IEEE Circuits & Systems Magazine*, with two goals in mind. First, we hope to bring important computational neuroscience research topics to the attention of *Circuits & Systems* researchers, covering representative neural signal processing applications. Second, we would like to pinpoint the ongoing research challenges and welcome cross-disciplinary contributions from the CAS community. The rest of the paper is organized as follows. Section II presents an overview of neural recording and stimulation technologies. Section III uses many neuroscience examples to illustrate neural signal processing applications. Finally, we present some discussions and conclusion in Section IV.

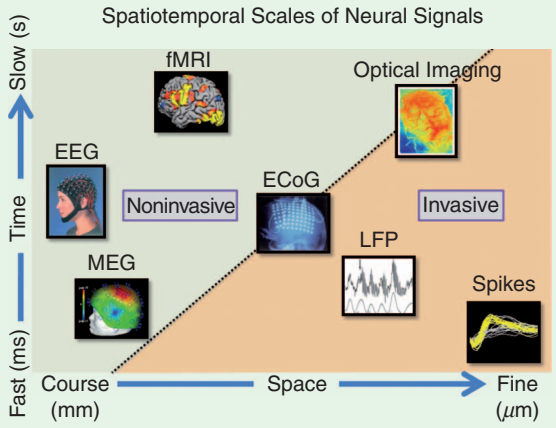

Figure 1. Comparison of invasive and non-invasive neural recordings with a wide range of temporal and spatial resolutions (figure courtesy of Dr. Nitish Thakor at Johns Hopkins University).

II. Advances in Neural Recording and Stimulation Technologies

Neuronal activity in the brain gives rise to transmembrane currents that can be measured in the extracellular medium [6]. For most invasive neural recordings, electrodes are implanted directly into the grey matter of brain (cortical or subcortical areas) such that high-fidelity neural signals are recorded with medium-to-high signal-to-noise ratio (SNR). Over the last five decades, progress in neural recording techniques has allowed the number of simultaneously recorded neurons to double approximately every seven

Table 1.
List of common types of neural signals.

Neural Signals	Physiological Measure
Spike trains	Measures high-pass filtered (>300 Hz) extracellular (discrete) action potentials of neurons
LFP (local field potential)	Measures low-pass filtered (<300 Hz) extracellular continuous signals in the vicinity of an electrode tip
EEG (electroencephalography)	Measures electric brain activity caused by the flow of electric currents during synaptic excitations of the dendrites in the neurons
MEG (magnetoencephalography)	Measures intracellular currents flowing through dendrites which produce magnetic fields that are measurable outside of the head
ECoG (electrocorticography)	Intracranial EEG recording from the surface of neocortex, with localized and higher spatial resolution
fMRI (functional magnetic resonance imaging)	Measures changes in local cerebral blood volume, cerebral blood flow and oxygenation levels induced from neural activation by electromagnetic fields
Calcium imaging	Measures dynamic calcium flux within neurons and neuronal tissue

Zhe Chen is with the Department of Psychiatry, Neuroscience and Physiology, School of Medicine, New York University, New York, NY, 10016 USA. E-mail: zhe.chen3@nyumc.org.

years, mimicking Moore's law [7]. Nowadays, various invasive or non-invasive recording and neuroimaging techniques have enabled us to record huge amount of spatial and temporal information from the functional brain *in vivo* (Table 1, Fig. 1). Development of high-density, multi-electrode recordings has been the trend, ranging from multi-electrode array (MEA), high-density adjustable microdrive, high-density silicon probe, to high-density electrocorticography (ECoG) or electroencephalography (EEG) recording

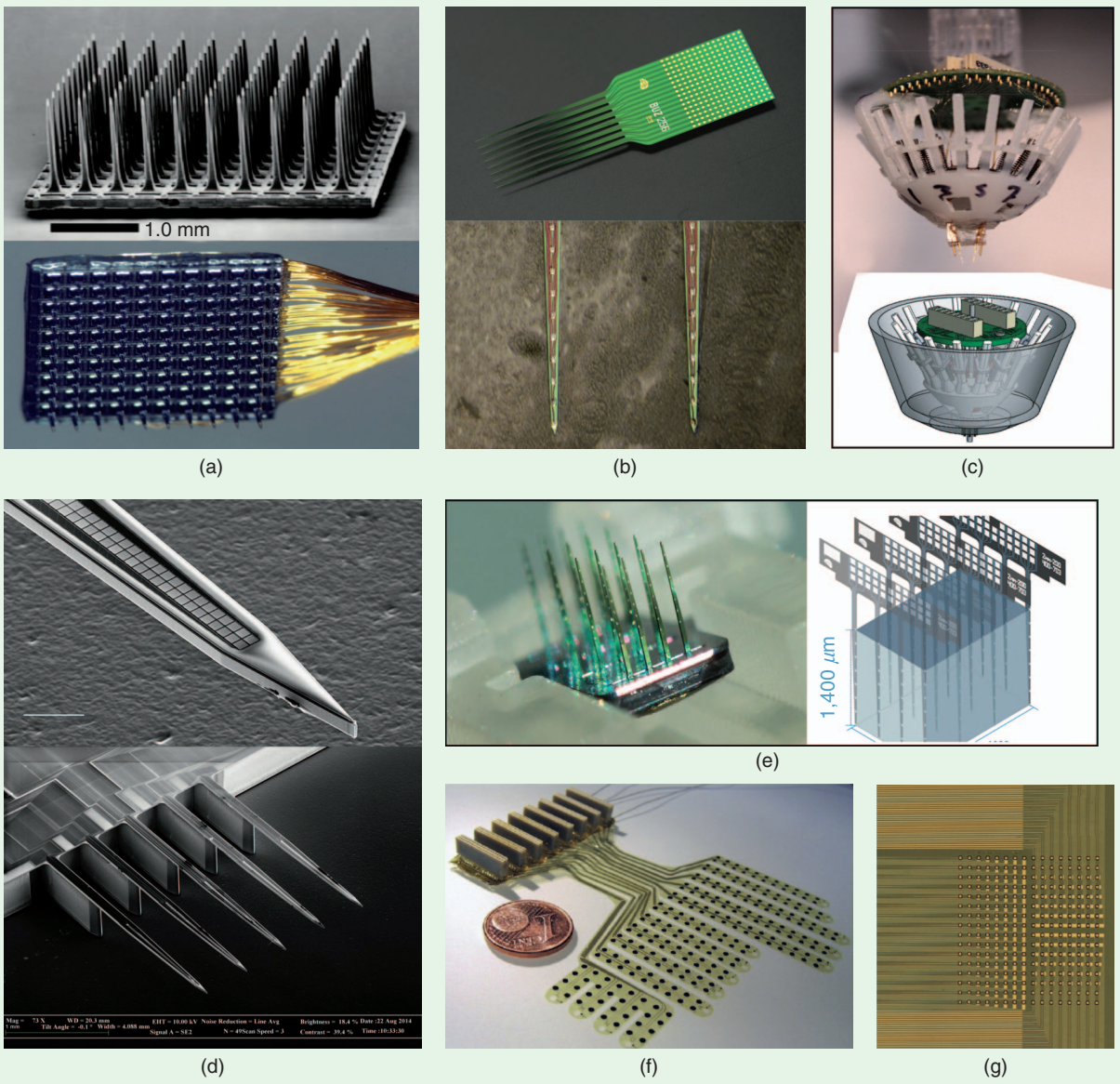

Figure 2. Illustrations of various electrodes for *in vivo* neurophysiological recordings. (A) Utah multielectrode (100-electrode) array (figure courtesy of Dr. John Donoghue at Brown University). (B) High-density silicon probe in rat hippocampal and neocortical recordings (figure courtesy of Dr. György Buzsáki at New York University) [8]. (C) A custom 96-channel high-density ultralight weight microdrive for mice (figure courtesy of Dr. Michael Halassa at New York University) [9]. (D) Closed-packed silicon microelectrodes consisting of 1000 electrode pads, each $9 \times 9\ \mu m^2$, at a pitch of $11\ \mu m$ (figure courtesy of Dr. Edward Boyden at Massachusetts Institute of Technology) [10]. (E) MatrixArray™ is a microfabricated silicon-based 3D electrode array that was developed to concurrently span cortical columns and layers providing a 3D interface to the nervous system. *Right:* MatrixArrays are comprised of multiple 2D arrays installed into a silicon platform with a pre-determined spacing (figure courtesy of Dr. Kazutaka Takahasi at the University of Chicago) [11]. (F) High-density 252-channel ECoG electrode grid with an optimized geometry for the left hemisphere of the macaque monkey brain. Note the arrangement of the grid in "fingers," allowing it to follow the curved surface of the brain [12] (reprinted with permission, © Elseiver, 2010). (G) 256-electrode NeuroGrid, where electrodes are $10 \times 10\ \mu m^2$ with 30-μm interelectrode spacing (figure courtesy of Dr. Dion Khodagholy at New York University) [13].

BOX 2: Spike sorting

Extracellular recordings are usually performed by inserting microwires into the brain. After amplification, the signal is low-pass filtered to obtain the LFP, and spikes are detected after high-pass filtering followed by an amplitude threshold. Features of the spike waveforms (such as the peak amplitude, energy, peak-to-trough width) are extracted and the spikes are sorted accordingly. Spikes with similar "clustered" features are grouped together into a "single-unit," which yields putative neuronal spike activity. In practice, manual or semi-automatic spike sorting procedures are used, followed by post-hoc neurophysiological analyses (e.g., inter-spike intervals, auto- and cross-correlogram). Non-stationary effects, such as temporal drifting in spike waveforms, appearance of new units, or disappearance of preexistent units, would make spike sorting very challenging.

system (Fig. 2). For a wide range of recorded neural signals, there is an intrinsic trade-off between spatial and temporal resolution. In this paper, due to space limitation we restrict our attention to the research using neural spike trains and EEG, while providing pointers to research areas based on other forms of neural signals.

In addition to neural recording techniques, neuroscience is also greatly empowered by new stimulation technologies, such as cell-type specific optogenetic stimulation [14], [15], deep brain stimulation (DBS) [16], and transcranial magnetic stimulation (TMS) [17]. Optogenetics is a biological technique which uses light to control *in vivo* neuronal activity in a temporally precise manner, thereby providing a powerful tool to investigate the causal and specific role of neural circuits in behavior [18]. DBS and TMS are two popular tools that are used in clinical practice to treat Parkinson's disease, depression, and other neurological disorders.

Together, advances in neural recording and stimulation technologies have enabled neuroscientists and engineers to design systems to understand, repair, replace, enhance, or otherwise exploit the properties of neural systems. Successful examples have included neuroprosthetics, brain-machine interface (BMI) and DBS, all of which rely on neural signal processing. In the next section, we will provide many case studies to illustrate the broad application of neural signal processing methods.

III. Neural Signal Processing

A. Preliminaries

1) Representation of Continuous Neural Signals

Continuous neural (e.g., LFP, EEG or imaging) signals are preprocessed to remove noise or artifact (based on filtering or sophisticated signal processing such as source separation). Due to high sampling rate, neural signals are temporally correlated. Multivariate continuous neural signals are often characterized by a zero-mean (multivariate) vector autoregressive (VAR) model. The parametric VAR model allows for inferring dynamic spectra, coherence, and Granger causality between neural signals [19].

2) Characterization of Neuronal Spikes

Action potentials, or spikes, are the fundamental signals by which neurons communicate and transmit information. Spikes are extracted from extracellular recordings by spike sorting (**BOX 2**). In continuous time, neural spike trains can be modeled as a point process with only 0/1 observations. Specifically, spike trains can be characterized by an instantaneous conditional intensity function (CIF) [20]:

$$\lambda(t) = \lim_{\Delta \to 0} \frac{\Pr\{\text{spike within time interval } [t, t+\Delta)\}}{\Delta} \quad (1)$$

The continuous-time point process is considered, approximately, to be a discrete-time binary time series. When the bin size Δ is sufficiently small, the product of $\lambda(t)\Delta$ is roughly equal to the instantaneous probability of spike occurrence. With a larger temporal bin size, spike trains can be binned into a time series with spike count observations. Popular probability distributions that characterize discrete count data include the binomial, Poisson, and negative binomial distributions.

Given $\lambda(t)$ $(0 \le t \le T)$, the point process log-likelihood is computed as [20]

$$\mathcal{L} = \int_0^T \log \lambda(t)\, dN(t) - \int_0^T \lambda(t)\, dt \quad (2)$$

where $dN(t) = 1$ in the presence of spike at time t, and 0 otherwise. In the case of discrete time bins, the integration is replaced by the summation. In this paper, we will use symbol t to refer to the continuous-time index, and use k for the discrete-time index (i.e., $t_k = k\Delta$).

B. Receptive Field Estimation

The receptive field (RF) of a neuron defines how its spiking activity changes in response to a stimulus. Characterizing neuronal RFs is a fundamental task to understand the neuronal tuning function in information representation. For instance, in visual systems, the neuronal tuning function is characterized by a 2D spatiotemporal RF;

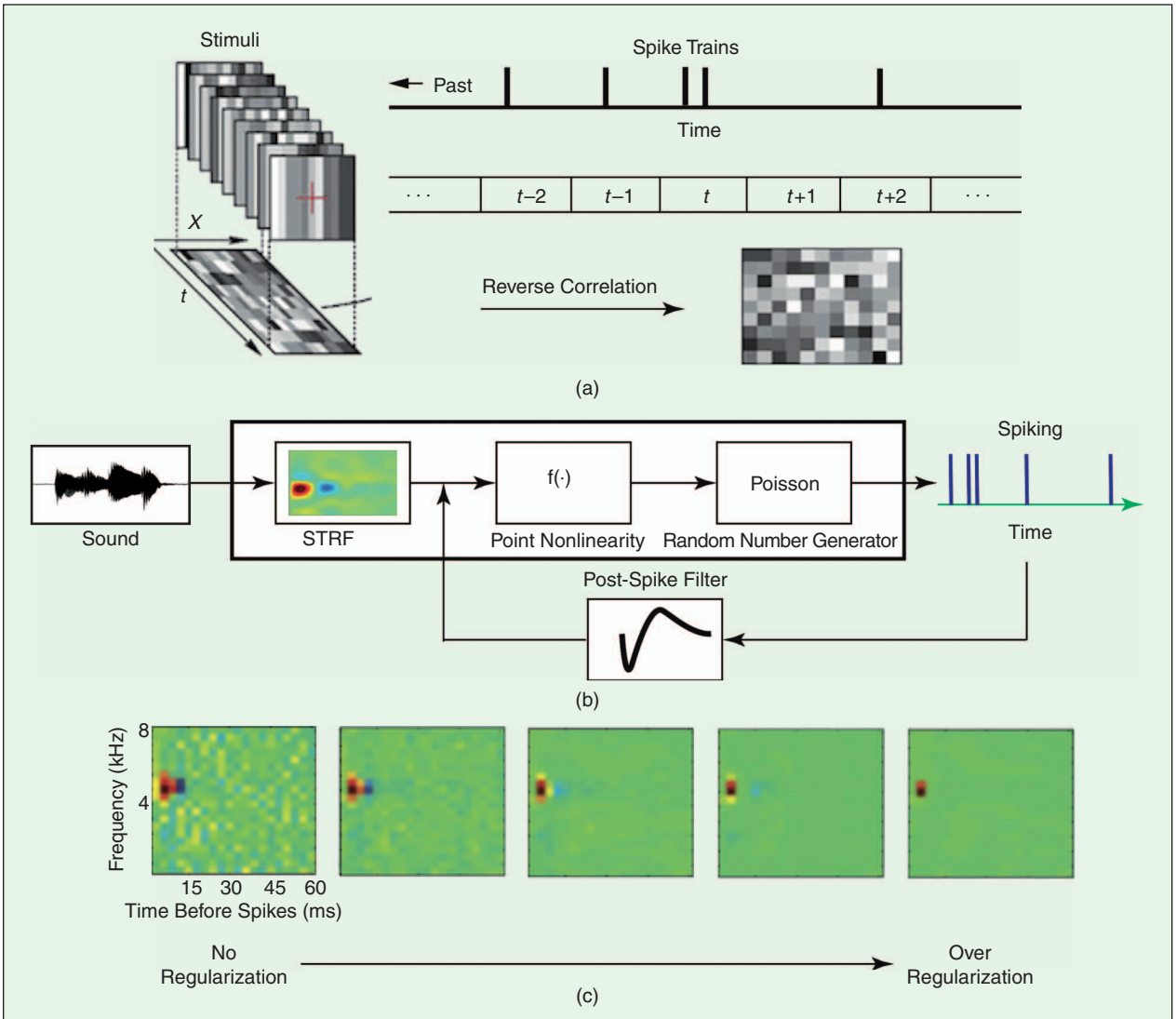

Figure 3. Models of neuronal receptive field. (A) Reverse correlation: the receptive field is estimated by regressed with spikes with temporally shifted stimuli using a linear Gaussian model. (B) A linear-nonlinear-Poisson (LNP) model for an auditory neuron. Each neuron has a stimulus filter or $\mathrm{STRF}(\tau,\omega)$, and a post-spike filter $h(l)$ that captures dependencies on the neuron's own spiking history. Summed filter output passes through a static nonlinearity $f(\cdot)$ to produce the instantaneous spike rate. (C) Illustration of the effect of a sparse prior on the STRF estimate. Panels from left to right show the STRFs estimated by penalized ML for increasing values of the regularization parameter. Low values of regularization lead to noisy estimates, and high values of regularization parameter lead to a sparse estimate (Adapted from [27] with permission).

whereas in auditory systems, it is characterized as a spectrotemporal RF (STRF). In the case of auditory neurons, the classic STRF model assumes a linear relationship between the time-dependent neuronal response $r(t_k)$ and the time-frequency spectrum of acoustic stimuli $s(k,\omega)$:

$$r(t_k) = r_0 + \sum_{\tau}\sum_{\omega} \mathrm{STRF}(\tau,\omega)\, s(k-\tau,\omega) \qquad (3)$$

where r_0 denotes the baseline firing rate, $s(k-\tau,\omega)$ denotes the stimulus energy at different tonotopic locations ω and different time delays $\tau > 0$. The strength and nature of the influences, whether being excitatory (positive) or suppressive (negative), is described by the STRF gain function $\mathrm{STRF}(\tau,\omega)$. In the early literature, the standard method for mapping the RF is *reverse correlation* [25]. The optimal solution (in least-squared sense) to equation (3) is given by the Wiener solution. When the stimulus is symmetric and white, the reverse correlation reduces to the spike-triggered average (STA) as a special case [26]. In order to characterize the response nonlinearity and non-Gaussianity and to account for the spiking history, a so-called linear-nonlinear Poisson (LNP) model has been developed (Fig. 3), which consists of a linear filter, followed by a pointwise static nonlinearity

BOX 3: Generalized linear models for modeling neuronal spike trains

The generalized linear model (GLM) is a class of statistical models that extend the original linear regression by allowing the response variables that have error distribution models other than a Gaussian distribution. The GLM is constructed by allowing the linear model to be related to the response variable via a link function (for instance, the canonical link function is 'log' for the Poisson and 'logit' for the binomial). For an exponential family, the natural parameter is a linear function of the predictors or covariates. GLMs have been used for modeling neural spike trains with either 0/1 observations or spike counts [21]–[23].

Statistical inference methods for GLM include the likelihood and Bayesian approaches. When a canonical link function is used, the maximum likelihood (ML) estimation of GLM can be reformulated as a convex optimization problem, which is solved efficiently by the iteratively reweighed least squares (IRWLS) or conjugate gradient optimization [2]. The goodness-of-fit of the point process GLM (ppGLM) can be assessed by the time-rescaling theorem and Kolmogorov-Smirnov (KS) test [24], as well as the predictive likelihood.

and a Poisson random number generator. At the fine timescale, the LNP model can be viewed as a generalized linear model (GLM; **Box 3**). Specifically, to account for non-Poisson spiking (such as the refractory period and bursting), one can incorporate a post-spike history filter and model the instantaneous firing rate as [27]

$$\lambda(t_k) = f\Bigg(\theta_0 + \sum_f \sum_\tau \underbrace{\mathrm{STRF}(\tau,\omega)s(k-\tau,\omega)}_{\text{stimulus effect}} + \sum_l \underbrace{h(l)n(k-l)}_{\text{spike-history effect}}\Bigg) \tag{4}$$

where θ_0 is a constant, $h(l)$ is a finite-length post-spike filter, $n(k-l)$ denotes the spike count in the previous l-th window before time index k, and $f(\cdot)$ is a static nonlinearity, which is can be an exponential: $f(u) = \exp(u)$, or $f(u) = \log(1+\exp(u))$, or a custom function (e.g., $f(u) = \exp(u)$ for $u \le 0$ and $f(u) = 1 + u + (u^2/2)$ for $u > 0$). Since the size of parameters is large, we may use regularization in penalized ML estimation and impose a smooth (spectrotemporal Laplacian) or sparse prior on the STRF [27], [28], where the regularization parameter is selected from cross-validation.

Example 1: Mapping V1 receptive fields. Identifying the neuronal RFs in primary visual cortex (V1) is critical for understanding how the early visual system represents and transmits visual information. The moving bar experiment is a classic paradigm pioneered by Hubel and Wiesel [29] for measuring the V1 neuronal RFs. Here, the spike activity from V1 neurons was recorded in awake macaque monkeys during the moving bar experiment (Fig. 4), in which a moving light bar stimulus was used in multiple orientations in multiple trials per direction presented in random order. In [30], a novel method was proposed to map visual RFs by tomographic reconstruction. The new method consists of three important steps: At the first step, characterize the neural spike activity with a ppGLM, taking into account of the non-Poissonian firing effect at a fine timescale. At the second step, integrate the ppGLM estimates at multiple directions with filtered back projection yields the RF's spatial tuning $f(x, y)$. At the third step, define the RF size and orientation tuning $g(\alpha)$ using a statistical criterion.

Let $h(x, y, \alpha|\theta) = f(x, y|\theta)g(\alpha|\theta)$ denote the RF function with a factorial form, where $f(x, y|\theta)$ and $g(\alpha|\theta)$ denote the spatial and orientation tunings under moving bar angle θ, respectively. Let $\mathcal{R}(f)[\theta]$ denote the Radon transform that specifies the sliced projection of $f(x, y)$ along the specific projection angle θ. To reconstruct $f(x, y)$, the inverse Radon transform is applied

$$f(x, y) = \mathcal{R}^{-1}\{\mathcal{R}(f)[\theta]\} = \mathcal{F}_2^{-1}\{\mathcal{F}_1\{\mathcal{R}(f)[\theta]\}\}, \tag{5}$$

where $\mathcal{F}_1$ and $\mathcal{F}_2$ denote the 1D and 2D Fourier transforms, respectively.

In Step 1, for the jth moving bar direction θ_j, we model the log CIF of the spiking activity as the sum of stimulus-evoked and spike history-dependent components

$$\log\lambda_j(t_k) = \underbrace{\sum_{i=1}^{M} \xi_{i,j}^{(B)}\mathcal{B}_i}_{\text{stimulus-evoked effect}} + \underbrace{\sum_{l=1}^{L} \xi_{l,j}^{(n)} n_{k-l,j}}_{\text{spike-history effect}} \tag{6}$$

where the first term consists of M basis functions that represent the stimulus-evoked component related to the RF characteristic, and the second term of spike history (spike counts up to preceding L windows) is related to the neuron's intrinsic biophysical property. The GLM coefficients $\{\xi_{i,j}^{(B)}, \xi_{l,j}^{(n)}\}$ can be estimated efficiently for each direction j. Due to circular geometry of the stimulus representation, the neuronal response along a moving bar angle θ_j is treated as a line integration of the 2D RF spatial tuning function $f(x, y)$ orthogonal to the moving direction. Therefore, we can approximate the Radon transform as

$$\hat{\mathcal{R}}(f)[\theta_j] = \exp\Bigg\{\sum_{i=1}^{M} \xi_{i,j}\mathcal{B}_i\Bigg\}, \tag{7}$$

Plugging (7) into (5) for all moving bar directions and applying filtered backprojection yields the estimate

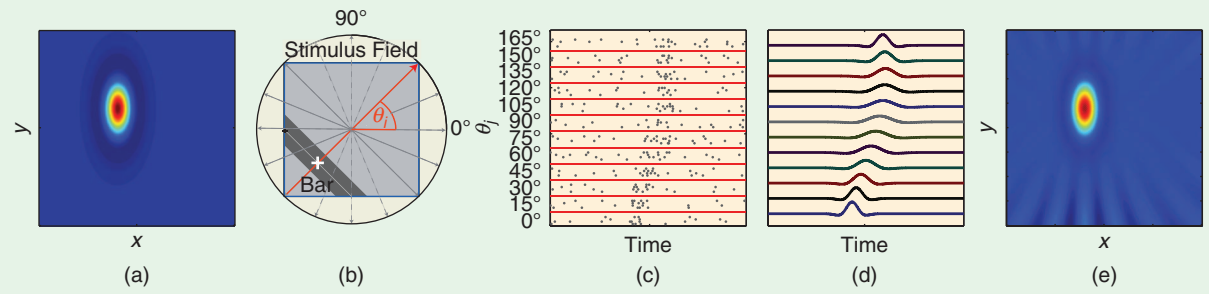

Figure 4. Mapping of V1 neuronal receptive fields by tomographic reconstruction. (A) 2D visual RF in the Cartesian coordinate (x, y) (warm shading represents high firing rate). (B) The bar is moved with a constant velocity with an angle θ_j across the rectangular visual field. (C) Raster plot of a single V1 neuron recorded from an awake monkey with respect to 12 moving bar directions; each row represents recording from one trial in one specific direction. (D) Estimated CIF profiles in 12 directions from panel C. (E) Reconstructed RF using filtered back projection based on the 12 estimates from panel D. (Adapted from [30] with permission, © MIT Press, 2012).

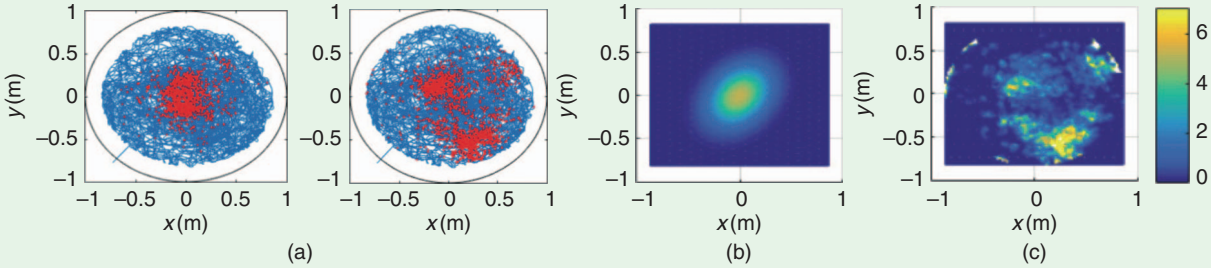

Figure 5. Estimating of place RFs in a 2D open field environment. (A) Spike activity of a unimodal place field (left) and a multimodal place field (right). Rat's run trajectory is marked by blue lines, and red dots mark the rat's spatial position when the cell spikes. (B) Unimodal place RF estimated by quadratic polynomials. (C) Multimodal place RF (color bar unit: spikes/s) estimated by a nonparametric kernel density estimator (Adapted from [32] with permission, © MIT Press, 2016).

$\hat{f}(x, y)$. See Fig. 4 for a schematic illustration. For details of Steps 2 and 3, see [30].

Example 2: Mapping place receptive fields. The hippocampus plays an important role in spatial navigation, episodic memory, learning and action planning. Pyramidal neurons in the hippocampus and entorhinal cortex exhibit spatial tuning during spatial navigation, and their place RFs characterize the neurons' spiking probability with respect to space. In a 2D spatial environment, it is referred to as a spatial function $\lambda(x, y) \geq 0$ in the Cartesian coordinate (x, y). For instance, the log-CIF function can be expressed by a linear sum of basis functions:

$$\log \lambda(t\,|x_t, y_t) = \sum_{i=1}^{M} \xi_i \mathcal{B}_i(x_t, y_t) \tag{8}$$

where $\{\mathcal{B}_i\}$ denotes a set of (quadratic or Zernike) polynomial basis functions [31], [32]. However, the parametric GLM in (8) is less flexible and insufficient to capture complex, multimodal RF. To account for the spike-history dependency, the CIF of neuronal spike trains can be written in the following form as the ratio of two densities [32], [33]

$$\begin{aligned}\lambda(t|\,x_t, y_t, h_t) &\approx \frac{N}{T}\frac{p(x_t, y_t, h_t\,|\,\text{spike})}{p(x_t, y_t, h_t)} \\ &= \frac{N}{T}\lambda(x, y)\frac{p_{H|X,Y,\text{spike}}(h_t)}{p_{H|X,Y}(h_t)}\end{aligned} \tag{9}$$

where h_t denotes the spike history at time t, N denotes the total number of spikes within total duration T, $p(x, y, h\,|\,\text{spike})$ denotes a 3D conditional pdf of spatial position and spike history conditioned on neuronal spiking, and the denominator $p(x, y, h) > 0$ denotes a 3D joint pdf of spatial position and spike history. In the second step of equation (9), $\lambda(x, y) \stackrel{\Delta}{=} (p_{X,Y\,|\,\text{spike}}(x, y)/p_{X,Y}(x, y))$, and the density ratio can be further estimated by applying change-of-variables and nonparametric density estimators [32]. Finally, we define the place RF as the expected value of $\lambda(x, y, h)$ with respect to the probability distribution of spike history $p_H(h)$: $\text{RF}(x, y) = \mathbb{E}_h[\lambda(x, y, h)]$.

Table 2.
Overview of neural decoding literature and representative references.

Brain Region	Use of Neural Signals
Monkey motor cortex	SUA [37]–[40], MUA [41], LFP [42]–[44]
Human motor cortex	SUA [45], MUA [46], LFP [47]
Monkey posterior parietal cortex	SUA [48], LFP [49]
Human posterior parietal cortex	fMRI [50]
Monkey retina	SUA [51], [52]
Monkey visual cortex	SUA [53]
Human visual cortex	fMRI [54]
Song bird auditory cortex	SUA [55]
Rodent hippocampus	SUA [31], [56], [57], MUA [33], LFP [58]

C. Neural Decoding

The goal of neural decoding is to construct sensory and other stimuli from information that has already been encoded in the neural signals derived from the brain. Neural signals may have the form of sorted single-unit activity (SUA), unsorted multi-unit activity (MUA), LFP, ECoG, EEG, MEG, or fMRI signals recorded from animals or humans (Table 2). Decoding approaches can be categorized into ML decoding and Bayesian decoding. The goal of Bayesian decoding is to estimate the posterior probability of signal of interest $\mathbf{x}$, given by the observed data $\mathbf{y}$. In light of Bayes' rule, we compute the posterior $P(\mathbf{x}|\mathbf{y})$ as follows [34]

$$P(\mathbf{x}|\mathbf{y}) = \frac{P(\mathbf{y}|\mathbf{x})P(\mathbf{x})}{P(\mathbf{y})} = \frac{P(\mathbf{y}|\mathbf{x})P(\mathbf{x})}{\int P(\mathbf{y}|\mathbf{x})P(\mathbf{x})d\mathbf{x}} \tag{10}$$

where $P(\mathbf{x}|\mathbf{y})$ denotes the likelihood, $P(\mathbf{x})$ denotes the prior, and $P(\mathbf{y})$ denotes the normalization constant. Neural signals are dynamic in time. To characterize the temporal relationship between spatiotemporal neural signals and behavior, we often formulate the decoding analysis within the framework of state space model (SSM) [1], [35]. The SSM consists of a state equation (11) that characterizes the evolution dynamics or transition probability of the latent state, and an observation equation (12) that describes the probability of the observed signals conditional to latent state.

$$\mathbf{x}_k = f(\mathbf{x}_{k-1}, \mathbf{w}_k) \quad \text{state equation for} \quad P(\mathbf{x}_k \mid \mathbf{x}_{k-1}) \tag{11}$$

$$\mathbf{y}_k = g(\mathbf{x}_k, \mathbf{v}_k) \quad \text{observation equation for} \quad P(\mathbf{y}_k \mid \mathbf{x}_k) \tag{12}$$

where $f(\cdot)$ and $g(\cdot)$ denote two generic functions, $\mathbf{w}_k$ and $\mathbf{v}_k$ denote the dynamic and measurement noise processes, respectively. Given observations $\mathbf{y}_{0:k}$ up to time index k, the the filtering posterior probability distribution of the state conditional on the observations $\mathbf{y}_{0:k}$ is [36]:

$$\begin{aligned} p(\mathbf{x}_k|\mathbf{y}_{0:k}) &= p(\mathbf{x}_k|\mathbf{y}_k, \mathbf{y}_{1:k-1}) \\ &= \frac{p(\mathbf{x}_k, \mathbf{y}_k, \mathbf{y}_{1:k-1})}{p(\mathbf{y}_k, \mathbf{y}_{1:k-1})} \\ &= \frac{p(\mathbf{y}_{1:k-1})p(\mathbf{x}_k, \mathbf{y}_k|\mathbf{y}_{1:k-1})}{p(\mathbf{y}_{1:k-1})p(\mathbf{y}_k|\mathbf{y}_{1:k-1})} \\ &= \frac{p(\mathbf{x}_k|\mathbf{y}_{0:k-1})p(\mathbf{y}_k|\mathbf{x}_k, \mathbf{y}_{1:k-1})}{p(\mathbf{y}_k|\mathbf{y}_{1:k-1})} \end{aligned} \tag{13}$$

The one-step state prediction, known as the *Chapman-Kolmogorov equation*, is

$$p(\mathbf{x}_k|\mathbf{y}_{1:k-1}) = \int p(\mathbf{x}_k|\mathbf{x}_{k-1})p(\mathbf{x}_{k-1}|\mathbf{y}_{1:k-1})d\mathbf{x}_{k-1} \tag{14}$$

From the perspective of neural decoding, equation (12) is characterized by neural encoding models, equations (13) and (14) are used for recursive neural decoding.

Example 3: Decoding primate M1 population activity. The primary motor cortex (M1) is an important brain area responsible for motor representation of different parts of body (e.g., hand, arm, fingers, legs and torso). Individual M1 neurons exhibit strong directional tuning, and population of M1 neurons can represent precise movement driven by a large class of tuning curves [59]. The downstream circuits may translate kinematically-coded signals into required combinations of muscle activation signals to generate movement [60].

Without loss of generality, let $\mathbf{x}_k = [x, y, v_x, v_y, a_x, a_y]_k^\top$ represent the hand kinematics vector that consists of (x, y)-position, (x, y)-velocity, and (x, y)-acceleration of the hand at time $t_k = k\Delta$ (where Δ denotes the temporal bin size), and let $\mathbf{y}_k$ denote a $C \times 1$ vector containing the firing rates at time t_k for C recorded neurons. The SSM can be formulated by as a linear dynamical system or Kalman filter [38]

$$\mathbf{x}_k = \mathbf{A}\mathbf{x}_{k-1} + \mathbf{w}_k \tag{15}$$

$$\mathbf{y}_k = \mathbf{C}\mathbf{x}_k + \mathbf{v}_k \tag{16}$$

where $\mathbf{A} \in \mathbb{R}^{6\times 6}$ and $\mathbf{C} \in \mathbb{R}^{C\times 6}$, and $\mathbf{w}_k \in \mathcal{N}(\mathbf{0}, \mathbf{Q})$ and $\mathbf{v}_k \in \mathcal{N}(\mathbf{0}, \mathbf{R})$ are two zero-mean Gaussian noise processes. Equation (15) is the state equation that characterizes the dynamics of hand kinematics, and equation (16) is the observation equation. Given $\{\mathbf{y}_{1:k}\}$, we can first use an expectation-maximization (EM) algorithm to infer the unknown system parameters and noise statistics $\{\mathbf{A}, \mathbf{C}, \mathbf{Q}, \mathbf{R}\}$, and then run an iterative Kalman filter to

estimate the hand kinematics $\{\hat{\mathbf{x}}_{k|k}\}$ and its covariance $\mathbf{P}_{k|k}$ as follows

$$\hat{\mathbf{x}}_{k|k} = \mathbf{A}\hat{\mathbf{x}}_{k-1|k-1} + \mathbf{K}_k(\mathbf{y}_k - \mathbf{C}\mathbf{A}\hat{\mathbf{x}}_{k-1|k-1}) \quad (17)$$

$$\mathbf{P}_{k|k-1} = \mathbf{A}\mathbf{P}_{k-1|k-1}\mathbf{A}^\top + \mathbf{Q} \quad (18)$$

$$\mathbf{K}_k = \mathbf{P}_{k|k-1}\mathbf{C}^\top(\mathbf{C}\mathbf{P}_{k|k-1}\mathbf{C}^\top + \mathbf{R})^{-1} \quad (19)$$

$$\mathbf{P}_{k|k} = (\mathbf{I} - \mathbf{K}_k\mathbf{C})\mathbf{P}_{k|k-1} \quad (20)$$

where $\mathbf{K}_k$ denotes the Kalman gain. In practice, it is insufficient to characterize the precise relationship between the kinematics $\mathbf{x}_k$ and neural activity $\mathbf{y}_k$ with a linear Kalman filter. To address this issue, one can augment the linear Kalman filter with latent states in neural representation [61]

$$\begin{pmatrix}\mathbf{x}_k\\ \mathbf{z}_k\end{pmatrix} = \mathbf{A}\begin{pmatrix}\mathbf{x}_{k-1}\\ \mathbf{z}_{k-1}\end{pmatrix} + \mathbf{w}_k \quad (21)$$

$$\mathbf{y}_k = \mathbf{C}\mathbf{x}_k + \mathbf{D}\mathbf{z}_k + \mathbf{v}_k \quad (22)$$

where $\mathbf{z}_k \in \mathbb{R}^m$ denotes the latent variable, $\mathbf{A} \in \mathbb{R}^{(6+m)\times(6+m)}$ and $\mathbf{D} \in \mathbb{R}^{C\times m}$. In this case, the neural activity $\mathbf{y}_k$ is influenced not only by the hand kinematics $\mathbf{x}_k$, but also by latent variable $\mathbf{z}_k$ that accounts for unobserved common input. Note that the above two linear models assume Gaussianity for both observations and states, a nonlinear GLM extension of the model is discussed in [62] to accommodate Poisson observations.

Thus far, we have assumed the neuronal activity and movement kinematics have zero time lag in the SSM. Since the M1 neuronal activity often leads ahead or lags behind the movement kinematics, it is common to choose time lags corresponding to multiples of the bin size [38], [63]. Optimal time lag can be determined by cross-validation or information-theoretic criteria. In this case, the firing rate $\mathbf{y}_k$ is defined accordingly in a time-shifted window. Figure 6 presents two M1 population decoding examples while monkeys performed a "pinball" task and a "pursuit tracking" task [38]. One can use the correlation coefficient and mean-squared error to assess the similarity between the actual and reconstructed kinematics trajectories.

Example 4: Decoding rat hippocampal population activity. Because of the spatial tuning of hippocampal place cells, many algorithms have been developed to reconstruct rat's position based on hippocampal population codes, some based on sorted spikes [31], [56], [57], some based on unsorted ensemble spikes [33], and other based on LFP [58]. In the standard spike sorting-based decoding approach (Fig. 7A), the procedure consists of encoding analysis (step 1) and decoding analysis (step 2). However, spike sorting is a complex and error-prone process, and it often discards many non-clustered spikes. To sidestep spike sorting, we may directly estimate the rate function. Specifically, we extract the peak amplitude ("features") from the spike waveform of detected spikes, and we further model the high-dimensional features observed in time as a time-homogeneous spatial-temporal Poisson process (STPP) or temporal marked point process [64]. The basic idea of decoding analysis on unsorted hippocampal spikes is to directly map the high-dimensional features (denoted by vector $\mathbf{a}$) to the animal's position (denoted by a scalar x in the 1D environment; see Fig. 7, B and C), in which the spike waveform features are treated as a proxy of the unit identity. Specifically, we model the Poisson rate function of STPP by a density ratio [33]:

$$\lambda(\mathbf{a}, x) = \frac{N}{T}\frac{p(\mathbf{a}, x \mid \text{spike})}{\pi(x)} \quad (23)$$

where N denotes the total number of spikes within total duration T, $p(\mathbf{a}, x|\,\text{spike})$ denotes the joint pdf, and $\pi(x)$ denotes the occupancy pdf of x during the recording period. From equation (23), we can derive the posterior distribution of animal's position given n spike events within a specific time interval Δ:

$$P(x|\,\mathbf{a}_{1:n}) \propto P(x)\prod_{i=1}^{n}\lambda(\mathbf{a}_i, x)e^{-\lambda(x)\Delta} \quad (24)$$

where $\lambda(x) = (N/T)(p(x|\,\text{spike})/\pi(x))$ and $P(x)$ denotes the prior probability of animal's position (either temporal or spatial prior). The density functions $p(\mathbf{a}, x)$, $p(x)$ and $\pi(x)$ can be estimated by nonparametric statistical methods, such as kernel density estimation (KDE) and band-limited maximum likelihood (BLML) methods [32], [33]. Finally, we compute the MAP estimate given the posterior distribution (24).

D. Change-Point Detection

The purpose of change-point detection is to identify times when the probability distribution of a stochastic process or time series changes. It not only concerns detecting whether or not a change has occurred, but also identifying the times of any such changes. The change may be related to the statistical properties of the stochastic process, such as the mean, variance, correlation statistics, or spectral density. Neuroscience applications of such include detecting epileptic seizures [66], detecting changes in neural ensemble activity [67], or monitoring alertness of the brain [68].

Example 5: Detecting acute thermal pain signals. Pain is defined as an unpleasant sensory and emotional experience associated with actual or potential tissue damage,

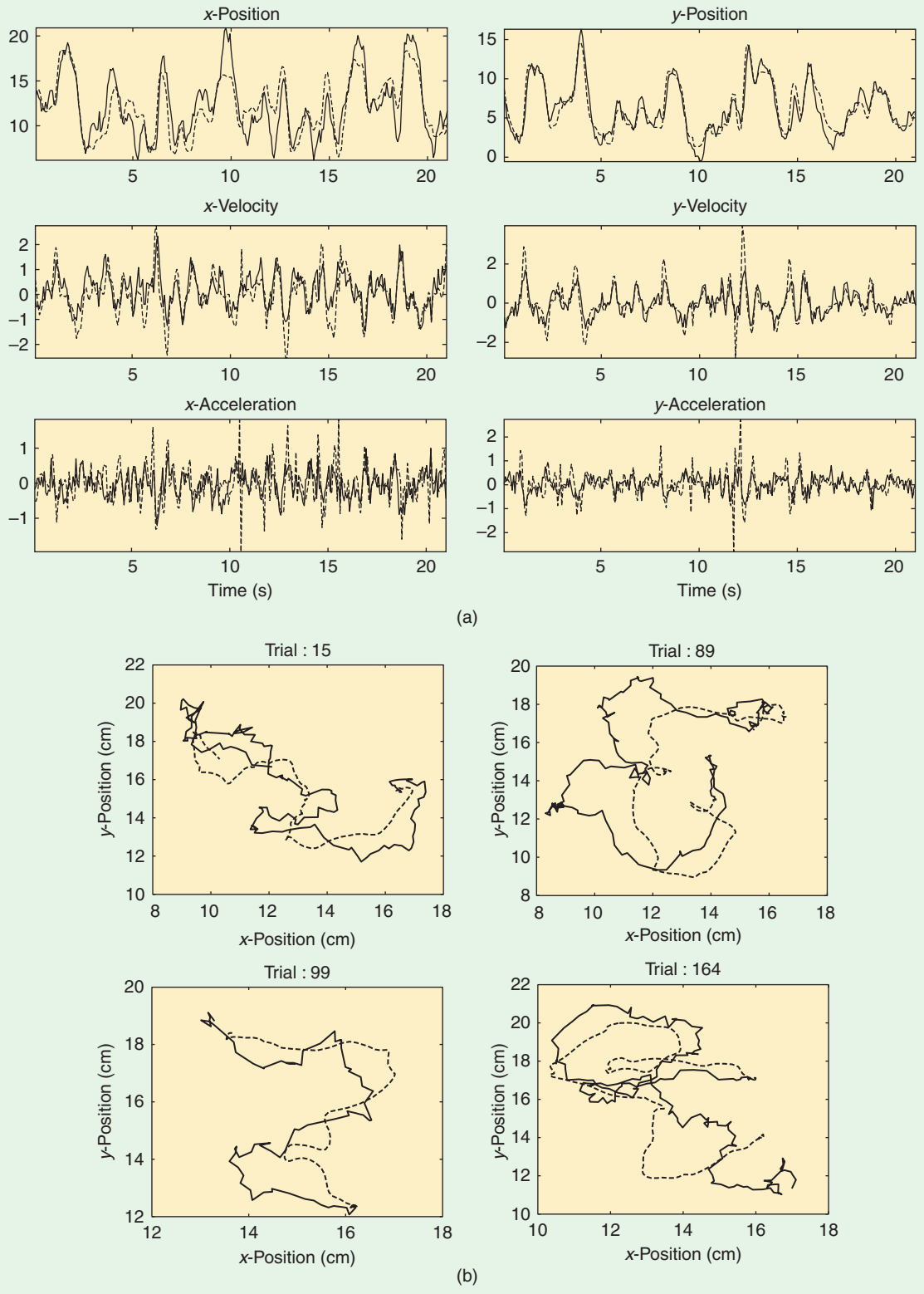

Figure 6. Decoding M1 population activity. (A) Pinball task. Reconstruction of 6-dimensional kinematic state: true (dashed) and reconstructed (solid) kinematic variables. Only 21 s of test sequence are shown. (B) Pursuit tracking task. Reconstruction of hand position on a few test trials: true (dashed) and reconstructed (solid) hand trajectories. (Adapted from [38] with permission, © MIT Press, 2005). (Figure courtesy of Dr. Wei Wu at Florida State University).

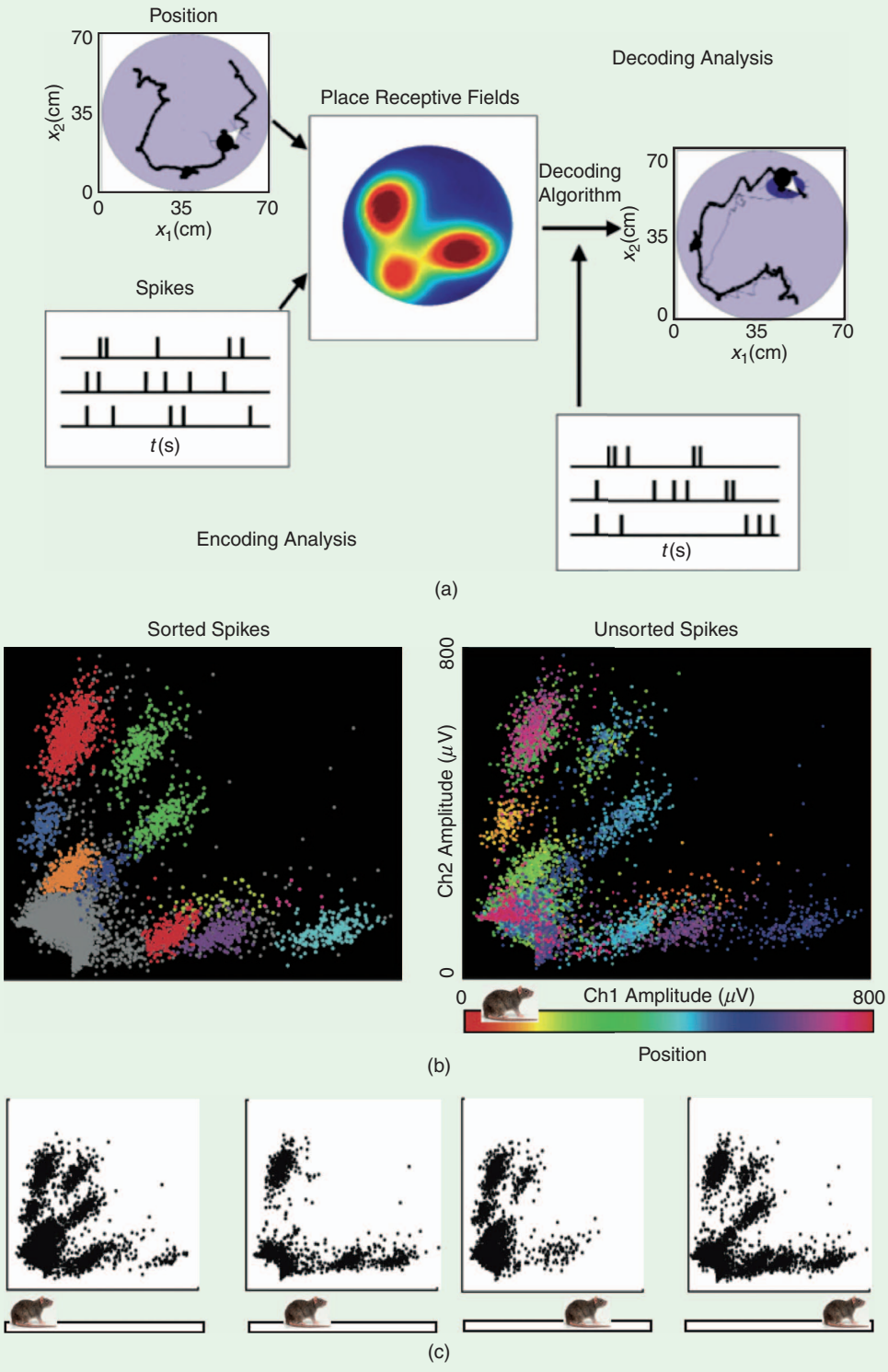

Figure 7. Reconstruction of rat's position from hippocampal population codes. (A) Schematic diagram of traditional hippocampal population decoding based on sorted spikes, which consists of encoding and decoding phases (Adapted from [65] with permission, © Nature Publisher Group, 2004). (B) Illustration of decoding unsorted ensemble spikes by relating the spatiotemporal ensemble spike patterns (using peak amplitudes from 2 electrode channels) to the rat's position (right), with color associated with different spatial position. For comparison, the same data but with sorted spikes are illustrated in the left panel, with each color representing a unique place cell identity. (C) Snapshots of distinct unsorted hippocampal ensemble spike patterns at different spatial locations, which will be characterized by the joint probability density $p(\mathbf{a},x)$. In this case, the rate function $\lambda(\mathbf{a},x)$ of the STPP is directly estimated from equation (23) without use of spike sorting [33].

or described in terms of such damage. Neuroimaging studies have identified circuit changes in the primary somatosensory cortex (S1) and anterior cingulate cortex (ACC) during pain states. The use of multielectrode arrays have enabled us to record many neurons from the S1 and ACC in freely behaving rats during an experimental protocol of acute thermal pain [69]. In the experiment, a blue laser with various intensity levels (150–250 mW) was delivered to the rat's hind paw, contralateral to the S1 or ACC recording site. A central goal is to reliably detect the acute thermal pain signals encoded by ensemble S1 and/or ACC responsive neurons on a single-trial basis, in the application of pain assessment or modulation. Here, we formulate the decoding as as change-point detection problem, where the change point is induced by the acute pain signal.

Let $\mathbf{y}_k = [y_{1,k}, \ldots, y_{C,k}]^\top$ denote a C-dimensional neuronal population vector, with each element denote the observed neuronal spike count at the k-th time bin. Let the univariate latent variable $z_k \in \mathbb{R}$ represents the unobserved common input (e.g., pain stimulus) that drives the neuronal population firing. The data-driven model can be described by a latent-state Poisson linear dynamical system (PLDS) [69]

$$z_k = az_{k-1} + \epsilon_k \tag{25}$$

$$\eta_k = \mathbf{c}z_k + \mathbf{d} \tag{26}$$

$$\mathbf{y}_k \sim \text{Poisson}(\exp(\eta_k)\Delta) \tag{27}$$

where state equation (25) is a first-order autoregressive (AR) model driven by a zero-mean Gaussian noise process $\epsilon_k \in \mathcal{N}(0, \sigma^2)$. The parameters $\mathbf{c}, \mathbf{d}$ or η_k are unconstrained; Δ denotes the temporal bin size. In [69], we developed an EM algorithm to estimate the smoothed posterior of $\hat{z}_{k|T}$ as well as the unknown parameters $\{a, \mathbf{c}, \mathbf{d}, \sigma\}$. From the estimated latent state $\hat{z}_{k|T}$, we further compute the Z-score related to the baseline: Z-score = (z-mean of z_{baseline}/SD of z_{baseline}). Under the assumption that the Z-score is standard normally distributed, we convert it to the one-tailed P-value:

$$\begin{aligned} P(\text{Z-score} > \hat{z}_{k|T}) &= 1 - P(\text{Z-score} \le \hat{z}_{k|T}) \\ &= 1 - \int_{-\infty}^{\hat{z}_{k|T}} \frac{1}{\sqrt{2\pi}} e^{\frac{-u^2}{2}} du \end{aligned} \tag{28}$$

The criterion of Z-score change (or equivalent P-value) is determined by a critical threshold for reaching statistical significance. For instance, using the significance criterion with one-sided P-value 0.05, it is concluded that when Z-score > 1.65 or Z-score < -1.65. In a quasi-stationary environment, once the model parameters are identified, we can derive a forward filter to recursively estimate the state variable

$$\hat{z}_{k|k-1} = a\hat{z}_{k-1|k-1} \tag{29}$$

$$Q_{k|k-1} = a^2 Q_{k-1|k-1} + \sigma^2 \tag{30}$$

$$\hat{\mathbf{y}}_{k|k-1} = \exp(\mathbf{c}\hat{z}_{k|k-1} + \mathbf{d})\Delta \tag{31}$$

$$Q_{k|k}^{-1} = Q_{k|k-1}^{-1} + \mathbf{c}^\top \text{diag}(\hat{\mathbf{y}}_{k|k-1})\mathbf{c} \tag{32}$$

$$\hat{z}_{k|k} = \hat{z}_{k|k-1} + Q_{k|k}\mathbf{c}^\top(\mathbf{y}_k - \hat{\mathbf{y}}_{k|k-1}) \tag{33}$$

where $Q_{k|k-1}$ and $Q_{k|k}$ denote the variance for predicted and filtered state, respectively.

In Fig. 8, we present a representative example of single-trial decoding analysis of S1 neuronal population (12 units) from a freely moving rat under 150 mW laser stimulation. As seen in the figure, the model-derived Z-score trace (blue) was much smoother than the empirical Z-score trace (computed from the raw spike count). Therefore, this model successfully detects the "neuronal threshold for acute pain" in the rat S1 population.

E. Brain-Machine Interface

The goal of BMI research is to create links between the nervous system and the external world by either stimulating or recording from neural tissue to treat or assist people with sensory, motor, or other disabilities of neural function [70]. The basic BMI research consists of two parts: open-loop prediction (i.e., reviewed in Section *III.D. Neural decoding*) and closed-loop control [40], [71]. The latter requires real-time processing for the purpose of neurofeedback (Fig. 9). The form of control or actuator can be a form of neural prosthetic device [70] or deep-brain stimulation (DBS) [72], or optogenetic control [73]. BMI systems can use invasive signals, such as neural spike trains and LFP [46], [47], or use non-invasive (or partially invasive) signals, such as scalp EEG or ECoG recordings [74] (Table 3). The complete BMI system consists of several stages: *signal acquisition, preprocessing and enhancing, feature extraction, signal processing*, and *control interface*. The key computational components are the last three stages. Depending on specific BMI designs, the computational task may include (i) classifying brain states; (ii) detecting change in neural activity; (iii) reconstructing sensory stimuli or motor kinematics; or (iv) delivering control or stimulation signals.

Example 6: EEG-based motor imagery. Motor imagery is a common mental task that is being widely used among BCI research groups [78]. For motor imagery tasks, subjects are instructed to imagine themselves performing specific motor actions (e.g., hand, foot, tongue) without overt motor outputs. The underlying basis of using motor imagery as a BCI strategy is that it induces contralateral preponderant event-related desynchronization (ERD) or synchronization (ERS), which is referred to respective short-lasting amplitude attenuation or enhancement

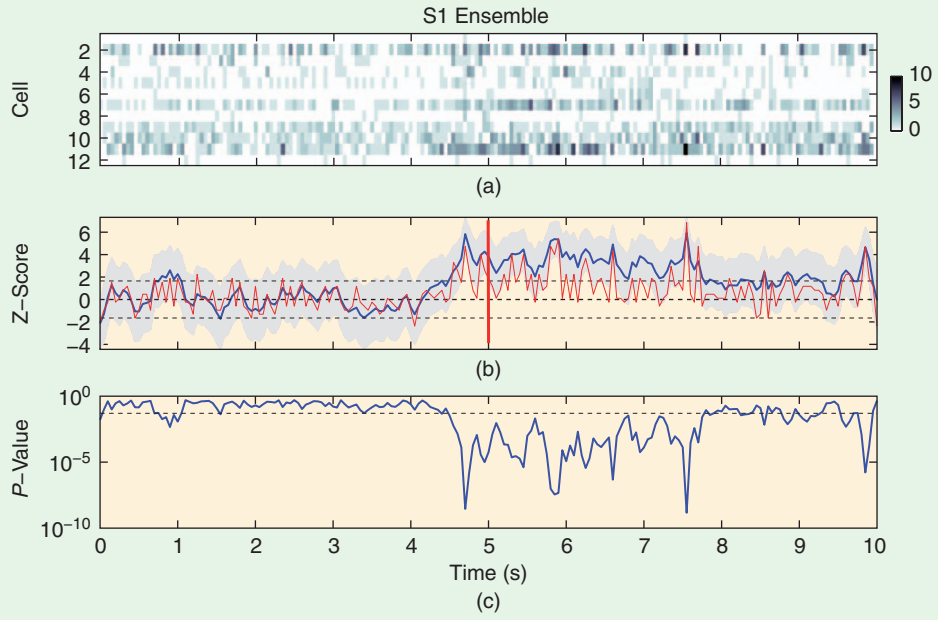

Figure 8. Detecting acute thermal pain signals. (A) neuronal ensemble spike counts (12 single units) from the rat S1 area. Bin size 50 ms. Color bar indicates spike count, with dark color representing high spike count. (B) Estimated mean Z-score (blue curve) from the smoothed state estimate $\hat{z}_{k|T}$. Vertical red line indicates the animal's paw withdrawal—an indicator of acute pain behavior. Horizontal dashed lines mark the thresholds of significant zone. Shaded area marks the confidence intervals. (C) Equivalent *P*-value derived from the mean Z-score (blue curve) of panel B (Adapted from [69], © IEEE, 2016).

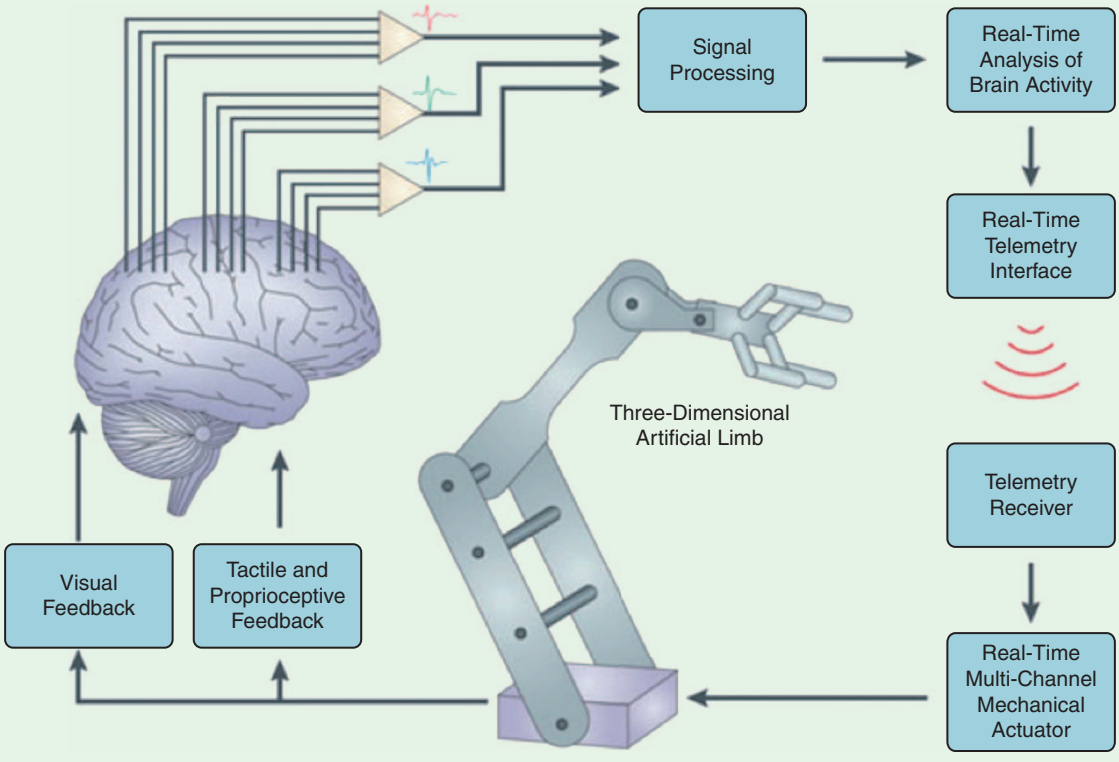

Figure 9. Closed-loop BMI control. Neuroprosthetics with various sensory feedbacks [75] (reprinted with permission, © Nature Publisher group, 2009). Because of the need of closed-loop control, real-time neural signal processing and analysis of brain activity are important elements in the BMI.

Table 3.
Overview of EEG or ECoG-based BMI systems.

Paradigm	Neural Correlate
Motor imagery	Event-related desynchronization and synchronization (ERD, ERS) of sensorimotor rhythms [76], [77]
Motor imagery	Slow cortical potentials (SCPs) [78]
Evoked potentials	Steady-state visual evoked potentials (SSVEPs), auditory steady state responses (ASSRs) [79]
Event-related potentials	P300, N200 [80], [81]

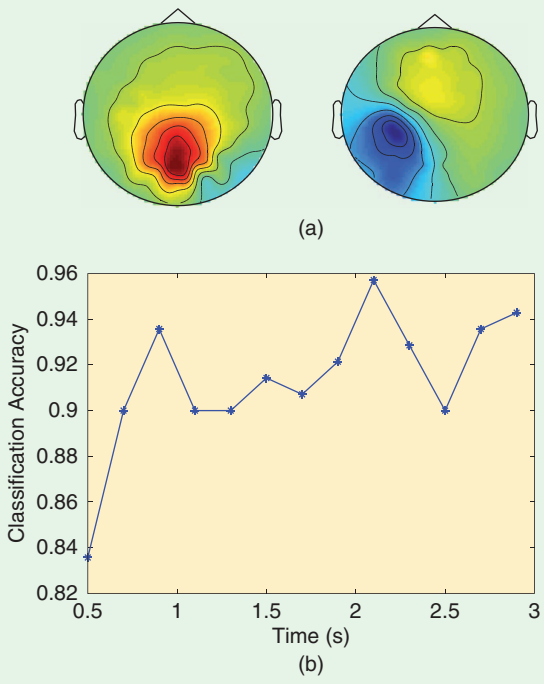

Figure 10. Application of the CSP algorithm in an EEG-based BMI system. (A) Topographies of extracted common spatial patterns: left hand (*left*) and foot (*right*). (B) Simulated online single-trial classification performance of motor imagery EEG data, time 0 indicates the cue onset. (Figure courtesy of Dr. Wei Wu at Stanford University.)

in the μ-rhythm (8–12 Hz) or beta-rhythm (14–30 Hz) components of EEG [76], [77]. Typically, the human motor imagery-based BMI system consists of preprocessing, feature selection, real-time classification (such as the Fisher linear discriminant analysis or linear support vector machine). Finding robust EEG spatiotemporal features for each subject is the key for the success of such BMI systems.

Learning common EEG components that distinguish different conditions is an effective feature extraction strategy for brain state classification. The common spatial patterns (CSP)-type algorithm [82], [83], which finds common EEG components with the largest variance ratios between two conditions, has attracted considerable attention. Let $\mathbf{X}^{(m)} \triangleq [\mathbf{x}_{:,1}^{(m)}, \ldots, \mathbf{x}_{:,L}^{(m)}]$ denote the EEG data matrix for m-th condition, which consists of the vectors of N-channel EEG signals with L sample points. Without loss of generality, we assume that the EEG signal at each channel have a zero mean. The objective of the CSP algorithm is to find a set of linear transformations (*spatial filters*) that maximizes the ratio of the transformed data's variance between two conditions:

$$\max_{\mathbf{w}} J(\mathbf{w}) = \frac{\mathbf{w}^\top \mathbf{R}^{(m)} \mathbf{w}}{\mathbf{w}^\top \mathbf{R}^{(m)} \mathbf{w}} \quad \text{s.t } \|\mathbf{w}\|_2 = 1 \tag{34}$$

where $\mathbf{w} \in \mathbb{R}^N$ denotes the spatial filter, and $\mathbf{R}^{(m)} = (1/L)\mathbf{X}^{(m)}(\mathbf{X}^{(m)})^\top$ denotes the sample spatial covariance matrix for condition k. Maximization of the Rayleigh quotient $J(\mathbf{w})$ can be formulated as the solution to a generalized eigenvalue problem: $\mathbf{R}^{(m)}\mathbf{w} = \lambda \mathbf{R}^{(m)}\mathbf{w}$, where λ denotes the eigenvalue associated with the eigenvector $\mathbf{w}$. However, this naive CSP solution is known to suffer from overfitting, which yields poor generalization performance. Instead, we can construct a probabilistic generative model and derive a Bayesian solution [5], [84], [85]. Specifically, we assume the following linear Gaussian model for EEG signal $\mathbf{X}$ at time k

$$\mathbf{X}_k^{(m)} = \mathbf{A}\mathbf{Z}_k + \mathbf{W}_k^{(m)} \tag{35}$$

$$\mathbf{Z}_k^{(m)} \sim \mathcal{N}(0, \mathbf{\Lambda}), \ \mathbf{W}_k^{(m)} \sim \mathcal{N}(0, \mathbf{\Sigma}) \tag{36}$$

What employs a common mixing matrix $\mathbf{A}$ between different conditions, where $\mathbf{\Lambda}$ and $\mathbf{\Sigma}$ denote the covariance matrices for Gaussian latent variable $\mathbf{Z}$ and Gaussian noise $\mathbf{W}$ (assumed to be temporally uncorrelated), respectively.

As an illustration, we apply the CSP algorithm to 118-channel EEG recording from one human subject. The subject was instructed to perform motor (left hand vs. foot) imagery experiments. The EEG signals were downsampled with 250 Hz and then bandpass filtered between 8 and 30 Hz. With a total of 140 trials for each class, 50% trials are used for training, and the remaining 50% trials are reserved for testing. Furthermore, 32 channels of relevance are selected for computing the features. Upon training (temporal window 0.5–3.5 s), the spatial patterns are shown in Fig. 10A. To simulate an online BMI setup, we also compute the classification rate curve across time using a moving window. We use the probabilistic CSP for feature extraction, and Fisher linear discriminant analysis for binary classification. Classification is performed every 200 ms based on the EEG signals in the previous time window of 500 ms. Each

How can we extract latent structures of large-scale neuronal ensemble spike trains, and how can we exploit sparsity or compressed sensing and apply them to neural signal processing?

point on the curve is obtained by calculating the mean classification rate within 140 trials at the corresponding time (Fig. 10B). In this example, the peak classification accuracy reaches around 96% around 2 seconds after the cue onset.

F. Other Research Topics

The topic of neural signal processing is very broad, therefore it is nearly impossible to cover every aspect or all technical details in this tutorial. In addition to the reviewed applications and examples, we briefly mention a few other important research topics below.

- *Inverse problems:* Applications include solving MEG or EEG inverse problems [86], deconvolving fMRI time series [87], and deconvolving spike trains from calcium imaging data [88]–[91].
- *Multimodal information fusion:* Examples include multimodal integration of MEG, EEG and fMRI recordings [92], [93], integration of optical neuromodulation and electrical recording [94].
- *Clinical and translational applications:* Examples include clinical BMI system [46], [95], DBS [96] and detection of epileptic seizures [97]–[99].
- *Data smoothing, dimensionality reduction and visualization:* Data smoothing and high-dimensional data visualization has become an increasingly important topic in neuroscience [100]. Many interesting questions arise: How can we extract meaningful information from limited high-dimensional spatiotemporal neural data from? How can we extract latent structures of large-scale neuronal ensemble spike trains [101], [102], and how can we exploit sparsity or compressed sensing and apply them to neural signal processing [103]–[105]?

IV. Discussion and Conclusion

In this paper, we provide a brief tutorial on neural signal processing. Due to space limitation, we cannot cover all aspects of this fast-growing field. Instead, we focus on a few important and representative applications along with illustrated examples. We also provide pointers to the state-of-the-art research in specific areas. In addition, some resources related to neural signal processing are listed in Table 4.

Despite rapid development and progresses in this emerging field, many challenges still remain. Here we would like to pinpoint a few challenges that particularly

Table 4.
Resources related to neural signal processing.

Resources	
Book	R. E. Kass, U. T. Eden and E. N. Brown, *Analysis of Neural Data*, Springer, 2015
	K. Oweiss, ed. *Statistical Signal Processing for Neuroscience and Neurotechnology*, Elsevier, 2010
	P. P. Mitra and H. Bokil, *Observed Brain Dynamics*, Oxford University Press, 2008
	M. X. Cohen, *Analyzing Neural Time Series Data: Theory and Practice*, MIT Press, 2014
	M. A. Kramer and U. T. Eden, *Case Studies in Neural Data Analysis: A Guide for the Practicing Neuroscientist*, MIT Press, 2016
	S. Sanei and J. A. Chambers, *EEG Signal Processing*, Wiley, 2007
Software	Spike sorting, https://github.com/magland/mountainlab
	http://klusta.readthedocs.io/en/latest/sorting/
	http://www2.le.ac.uk/departments/engineering/research/bioengineering/neuroengineering-lab/spike-sorting
	neural spike train analysis toolbox, www.neurostat.mit.edu/nstat
	spectral analysis of neural data, http://chronux.org/
	EEGLAB, http://sccn.ucsd.edu/eeglab/
	statistical parametric mapping (SPM) for fMRI data, http://www.fil.ion.ucl.ac.uk/spm/
	calcium imaging deconvolution, https://github.com/epnev/ca_source_extraction/blob/master/README.md
	Granger causality analysis, http://www.dcs.warwick.ac.uk/~feng/causality.html
	dimensionality reduction and visualization, https://users.ece.cmu.edu/~byronyu/software.shtml

welcome new contributions from the *Circuits and Systems* community. First, development of new theories and models for tackling large-scale neural recordings with complex or dynamic structure (such as non-stationarity, non-Gaussianity, hierarchy and mixed modality, sparsity). Nonparametric statistical methods may be valuable along this direction [106]. Second, development of computationally-efficient signal processing algorithms for large-scale neuoimaging data [91] and high-density multielectrode recordings [107], [108]. Third, development of embedded systems in signal processing or control components for closed-loop BMI systems [109]–[111]. Fourth, development of efficient wireless neural recording technologies for freely behaving animals [112]–[114].

In conclusion, neural signal processing plays an increasingly important role in neuroscience and neural engineering applications. With the advancement of neural recording and stimulation techniques, it becomes critical to develop computationally-efficient algorithms to tackle large-scale, high-dimensional neural signals. More research in new-generation embedded systems suitable for neural signal processing is anticipated in the near future.

Acknowledgment

The author would like to thank the former and current colleagues for their contributions cited in this paper, and thank L. Citi (University of Essex), J. Dauwels (Nanyang Technological University), K. Takahashi (University of Chicago), W. Wu (Stanford University) and W. Wu (Florida State University) for valuable feedback. The author also thanks the permission of using published figures from previous publishers. The work was supported by an NSF-CRCNS award (IIS-1307645 and 1443032) from the US National Science Foundation and an NIH-CRCNS award (R01-NS100065) from the National Institute of Neurological Disorders and Strokes (NINDS).

Zhe Chen received the Ph.D. degree in electrical and computer engineering in 2005 from McMaster University, Canada. Previously, He was a research scientist in the RIKEN Brain Science Institute (2005–2007) and a senior research scientist in Harvard Medical School and MIT (2007–2014). Currently, he is an Assistant Professor at the New York University School of Medicine, with joint appointment at the Department of Psychiatry and Department of Neuroscience and Physiology. His research interests include computational neuroscience, neural engineering, neural signal processing, machine learning, and Bayesian statistics. He is the lead author of the book *Correlative Learning* (Johns Wiley & Sons, 2007) and the editor of the book *Advanced State Space Methods for Neural and Clinical Data* (Cambridge University Press, 2015). He is a Senior Member of the IEEE and the action editor of *Neural Networks* (Elsevier). Dr. Chen has received a number of fellowship and awards, and is the lead principal investigator for two CRCNS (collaborative research in computational neuroscience) awards funded by the National Science Foundation (NSF) and National Institutes of Health (NIH). His article has won the 2012 Brain Corporation Prize in Computational Neuroscience (3rd place).

References

[1] Z. Chen, R. Barbieri, and E. N. Brown, "State-space modeling of neural spike train and behavioral data," in *Statistical Signal Processing for Neuroscience and Neurotechnology*, K. Oweiss, Ed. *Amsterdam, The Netherlands*: Elsevier, 2010, pp. 175–218.

[2] Y. Pawitan, *In All Likelihood: Statistical Modeling and Inference Using Likelihood*. U.K.: Clarendon Press, 2001.

[3] C. P. Robert, *The Bayesian Choice: From Decision-Theoretic Foundations to Computational Implementation*, 2nd ed. *New York*: Springer-Verlag, 2007.

[4] J. V. Candy, *Bayesian Signal Processing: Classical, Modern and Particle Filtering Methods*. New York: Wiley, 2009.

[5] W. Wu, S. Nagarajan, and Z. Chen, "Bayesian machine learning: EEG/MEG signal processing measurements," *IEEE Signal Process. Mag.*, vol. 33, no. 1, pp. 14–36, 2016.

[6] G. Buzsáki, C. A. Anastassiou, and C. Koch, "The origin of extracellular fields and currents–EEG, ECoG, LFP and spikes," *Nature Rev. Neurosci.*, vol. 13, pp. 407–420, 2012.

[7] I. H. Stevenson and K. P. Kording, "How advances in neural recording affect data analysis," *Nature Neurosci.*, vol. 14, pp. 139–142, 2011.

[8] G. Buzsáki, E. Stark, A. Berényi, D. Khodagholy, D. R. Kipke, E. Yoon, and K. D. Wise, "Tools for probing local circuits: High-density silicon probes combined with optogenetics," *Neuron*, vol. 86, pp. 92–105, 2015.

[9] P. M. Bruentti, R. D. Wimmer, J. H. Siegle, J. Voigts, M. A. Wilson, and M. M. Halassa, "Design and fabrication of ultra-light weight, adjustable multi-electrode probes for electrophysiological recordings in mice," *J. Vis. Exp.*, vol. 91, pp. e51675, 2014.

[10] J. Scholvin, J. P. Kinney, J. G. Bernstein, C. Moore-Kochlacs, N. Kopell, C. G. Fonstad, and E. S. Boyden, "Close-packed silicon microelectrodes for scalable spatially oversampled neural recording," *IEEE Trans. Biomed. Eng.*, vol. 63, no. 1, pp. 120–130, 2016.

[11] K. Qian, K. Balasubramanian, N. G. Hatsopoulos, and K. Takahashi, "Laminar pattern classification of beta oscillation range of LFPs recorded from the motor cortex with a chronic 3D electrode array," in *Proc. IEEE Engineering Medicine and Biology Conf.*, 2015.

[12] A. Ritaccio, P. Brunner, M. C. Cervenka, N. Crone, et al., "The scientific explorations of epilepsy and behavior: Proceedings of the first workshop on advances in electrocorticography," *Epilepsy Behav.*, vol. 19, pp. 204–215, 2010,

[13] D. Khodagholy, J. N. Gelinas, T. Thesen, W. Doyle, O. Devinsky, G. G. Malliaras, and G. Buzsáki, "Neurogrid: Recording action potentials from the surface of the brain," *Nat Neurosci.*, vol. 18, pp. 310–315, 2015.

[14] E. S. Boyden, F. Zhang, E. Bamberg, G. Nagel, and K. Deisseroth, "Millisecond-timescale, genetically targeted optical control of neural activity," *Nature Neurosci.*, vol. 8, pp. 1263–1268, 2015.

[15] E. S. Boyden, "Optogenetics and the future of neuroscience," *Nature Neurosci.*, vol. 18, pp. 1200–1201, 2015.

[16] S. Miocinovic, S. Somayajula, S. Chitnis, and J. L. Vitek, "History, applications, and mechanisms of deep brain stimulation," *JAMA Neurol.*, vol. 70, no. 2, pp. 163–171, 2013.

[17] V. Walsh and A. Pascual-Leone, *Transcranial Magnetic Stimulation: A Neurochronometrics of Mind*. Cambridge, MA: MIT Press, 2003.

[18] K. M. Tye and K. Deisseroth, "Optogenetic investigation of neural circuits underlying brain disease in animal models," *Nature Rev. Neurosci.*, vol. 13, no. 4, pp. 251–266, 2012.

[19] A. K. Seth, A. B. Barrett, and L. Barnett, "Granger causality analysis in neuroscience and neuroimaging," *J. Neurosci.*, vol. 35, no. 8, pp. 3293–3297, 2015.

[20] E. N. Brown, "The theory of point processes for neural systems," in *Methods and Models in Neurophysics*, C. Chow, B. Gutkin, D. Hansel,

C. Meunier, and J. Dalibard, Eds. *Amsterdam, The Netherlands*: Elsevier, 2005, pp. 691–726.
[21] L. Paninski, "Maximum likelihood estimation of cascade point-process neural encoding models," *Network: Comput. Neural Syst.*, vol. 15, pp. 243–262, 2004.
[22] W. Truccolo, U. T. Eden, M. Fellow, J. P. Donoghue, and E. N. Brown, "A point process framework for relating neural spiking activity to spiking history, neural ensemble and covariate effects," *J. Neurophysiol.*, vol. 93, pp. 1074–1089, 2005.
[23] Z. Chen and E. N. Brown, "Generalized linear models for point processes analyses of neural spike activity," in *Encyclopedia of Computational Neuroscience*, D. Jaeger and R. Jung, Eds. *New York*: Springer-Verlag, 2015, pp. 1284–1287.
[24] E. N. Brown, R. Barbieri, V. Ventura, R. E. Kass, and L. M. Frank, "The time-rescaling theorem and its application to neural spike data analysis," *Neural Comput.*, vol. 14, pp. 325–346, 2002.
[25] D. Ringach and R. Shapley, "Reverse correlation in neurophysiology," *Cogn. Sci.*, vol. 28, pp. 147–166, 2004.
[26] O. Schwartz, J. W. Pillow, N. C. Rust, and E. P. Simoncelli, "Spike-triggered neural characterization," *J. Vision*, vol. 6, pp. 484–507, 2006.
[27] A. Calabrese, J. W. Schumacher, D. M. Schneider, L. Paninski, and S. M. N. Woolley, "A generalized linear model for estimating spectrotemporal receptive fields from responses to natural sounds," *PLoS ONE*, vol. 6, no. 1, pp. 1–16, 2011.
[28] C. K. Machens, M. S. Wehr, and A. M. Zador, "Linearity of cortical receptive fields measured with natural sounds," *J. Neurosci.*, vol. 24, no. 5, pp. 1089–1100, 2004.
[29] D. H. Hubel and T. N. Wiesel, "Receptive fields of single neurons in the cat's striate cortex," *J. Physiol.*, vol. 148, pp. 574–591, 1959.
[30] G. Pipa, Z. Chen, S. Neuenschwander, B. Lima, and E. N. Brown, "Mapping of visual receptive fields by tomographic reconstruction," *Neural Comput.*, vol. 24, no. 10, pp. 2543–2578, 2012.
[31] R. Barbieri, L. M. Frank, D. P. Nguyen, M. C. Quirk, V. Solo, M. A. Wilson, and E. N. Brown, "Dynamic analyses of information encoding in neural ensembles," *Neural Comput.*, vol. 16, no. 2, pp. 277–307, 2004.
[32] R. Agarwal, Z. Chen, F. Kloosterman, M. A. Wilson, and S. Sarma, "A novel nonparametric approach for neural encoding and decoding models of multimodal receptive fields," *Neural Comput.*, vol. 28, pp. 1356–1387, 2016.
[33] F. Kloosterman, S. P. Layton, Z. Chen, and M. A. Wilson, "Bayesian decoding using unsorted spikes in the rat hippocampus," *J. Neurophysiol.*, vol. 111, no. 1, pp. 217–227, 2014.
[34] Z. Chen, "An overview of Bayesian methods for neural spike train analysis," *Comput. Intell. Neurosci.*, vol. 2013, pp. 251905, 2013.
[35] Z. Chen, Ed., *Advanced State Space Methods in Neural and Clinical Data*. Cambridge, U.K.: Cambridge Univ. Press, 2015.
[36] Z. Chen and E. N. Brown, "State space model," *Scholarpedia*, vol. 8, no. 3, pp. 30868, 2013.
[37] A. E. Brockwell, A. L. Rojas, and R. E. Kass, "Recursive Bayesian decoding of motor cortical signals by particle filtering," *J. Neurophysiol.*, vol. 91, no. 4, pp. 1899–1907, 2004.
[38] W. Wu, Y. Gao, E. Bienenstock, J. P. Donoghue, and M. J. Black, "Bayesian population decoding of motor cortical activity using a Kalman filter," *Neural Comput.*, vol. 18, no. 1, pp. 80–118, 2006.
[39] B. M. Yu, C. Kemere, G. Santhanam, S. I. Ryu, T. H. Meng, M. Sahani, and K. V. Shenoy, "Mixture of trajectory models for neural decoding of goal-directed movements," *J. Neurophysiol.*, vol. 97, pp. 3763–3780, 2007.
[40] M. M. Shanechi, G. W. Wornell, Z. M. Williams, and E. N. Brown, "Feedback-controlled parallel point process filter for estimation of goal-directed movements from neural signals," *IEEE Trans. Neural Syst. Rehabil. Eng.*, vol. 21, pp. 129–140, 2013.
[41] A. K. Bansal, W. Truccolo, C. E. Vargas-Irwin, and J. P. Donoghue, "Decoding 3D reach and grasp from hybrid signals in motor and premotor cortices: Spikes, multiunit activity, and local field potentials," *J. Neurophysiol.*, vol. 107, pp. 1337–1355, 2012.
[42] L. Srinivasan, U. T. Eden, S. K. Mitter, and E. N. Brown, "General-purpose filter design for neural prosthetic devices," *J. Neurophysiol.*, vol. 98, pp. 2456–2475, 2007.
[43] J. Zhuang, W. Truccolo, C. Vargas-Irwin, and J. P. Donoghue, "Decoding 3-D reach and grasp kinematics from high-frequency local field potentials in primate primary motor cortex," *IEEE Trans. Biomed. Eng.*, vol. 57, no. 7, pp. 1774–1784, 2009.
[44] V. Aggarwal, M. Mollazadeh, A. G. Davidson, M. H. Schieber, and N. V. Thakor, "State-based decoding of hand and finger kinematics using neuronal ensemble and LFP activity during dexterous reach-to-grasp movements," *J. Neurophysiol.*, vol. 109, no. 12, pp. 3067–3081, 2013.
[45] W. Truccolo, G. M. Fiehs, J. P. Donoghue, and L. R. Hochberg, "Primary motor cortex tuning to intended movement kinematics in humans with tetraplegia," *J. Neurosci.*, vol. 28, no. 5, pp. 1163–1178, 2008.
[46] L. R. Hochberg, M. D. Serruya, G. M. Friehs, et al., "Neuronal ensemble control of prosthetic devices by a human with tetraplegia," *Nature*, vol. 442, pp. 164–171, 2006.
[47] J. A. Perge, S. Zhang, W. Q. Malik, et al., "Reliability of directional information in unsorted spikes and local field potentials recorded in human motor cortex," *J. Neural Eng.*, vol. 11, no. 4, pp. 0046007, 2014.
[48] G. H. Mulliken, S. Musallam, and R. A. Andersen, "Decoding trajectories from posterior parietal cortex ensembles," *J. Neurosci.*, vol. 28, no. 48, pp. 12913–12926, 2008.
[49] E. J. Hwang and R. A. Andersen, "Brain-control of movement execution onset using LFPs in posterior parietal cortex," *J. Neurosci.*, vol. 29, no. 45, pp. 14363–14370, 2009.
[50] T. Aflalo, S. Kellis, C. Klaes, et al., "Decoding motor imagery from the posterior parietal cortex of a tetraplegic human," *Science*, vol. 348, pp. 906–910, 2015.
[51] J. W. Pillow, J. Shlens, L. Paninski, A. Sher, A. M. Litke, E. J. Chichilnisky, and E. P. Simoncelli, "Spatio-temporal correlations and visual signalling in a complete neuronal population," *Nature*, vol. 454, pp. 995–999, 2008.
[52] A. L. Jacobs, G. Fridman, R. M. Douglas, N. M. Alama, P. E. Lathamd, G. T. Pruskya, and S. Nirenberga, "Ruling out and ruling in neural codes," *Proc. Natl. Acad. Sci. U.S.A.*, vol. 106, no. 14, pp. 5936–5941, 2009.
[53] A. B. A. Graf, A. Kohn, M. Jazayeri, and J. A. Movshon, "Decoding the activity of neuronal populations in macaque primary visual cortex," *Nature Neurosci.*, vol. 14, pp. 239–245, 2011.
[54] Y. Kamitani and F. Tong, "Decoding the visual and subjective contents of the human brain," *Nature Neurosci.*, vol. 8i, pp. 679–685, 2005.
[55] A. D. Ramirez, Y. Ahmadian, J. W. Schumacher, D. M. Schneider, S. M. N. Woolley, and L. Paninski, "Incorporating naturalistic correlation structure improves spectrogram reconstruction from neuronal activity in the songbird auditory midbrain," *J. Neurosci.*, vol. 31, no. 10, pp. 3828–3842, 2011.
[56] E. N. Brown, L. M. Frank, D. Tang, M. C. Quirk, and M. A. Wilson, "A statistical paradigm for neural spike train decoding applied to position prediction from ensemble firing patterns of rat hippocampal place cells," *J. Neurosci.*, vol. 18, no. 18, pp. 7411–7425, 1998.
[57] K. Zhang, I. Ginzburg, B. L. McNaughton, and T. J. Sejnowski, "Interpreting neuronal population activity by reconstruction: unified framework with application to hippocampal place cells," *J. Neurophysiol.*, vol. 79, no. 2, pp. 1017–1044, 1998.
[58] R. Agarwal, I. H. Stevenson, A. Berenyi, K. Mizuseki, G. Buzsaki, and F. T. Sommer, "Spatially distributed local fields in the hippocampus encode rat position," *Science*, vol. 344, no. 6184, pp. 626–630, 2014.
[59] A. P. Georgopoulos, A. B. Schwartz, and R. E. Kettner, "Neuronal population coding of movement direction," *Science*, vol. 233, pp. 1416–1419, 1986.
[60] A. E. Brockwell, R. E. Kass, and A. B. Schwartz, "Statistical signal processing and the motor cortex," *Proc. IEEE*, vol. 95, no. 5, pp. 881–898, 2007.
[61] W. Wu, J. E. Kulkarni, N. G. Hatsopoulos, and L. Paninski, "Neural decoding of hand motion using a linear state-space model with hidden states," *IEEE Trans. Neural Syst. Rehabil. Eng.*, vol. 17, pp. 370–378, 2009.
[62] V. Lawhern, W. Wu, N. G. Hatsopoulos, and L. Paninski, "Population decoding of motor cortical activity using a generalized linear model with hidden states," *J. Neurosci. Methods*, vol. 189, pp. 267–280, 2010.
[63] N. G. Hatsopoulos, Q. Xu, and A. Amit, "Encoding of movement fragments in the motor cortex," *J. Neurosci.*, vol. 27, no. 19, pp. 5105–5114, 2007.
[64] P. J. Diggle, Ed., *Statistical Analysis of Spatial and Spatio-Temporal Point Patterns*, 3rd ed. *Boca Raton, FL*: CRC, 2013.
[65] E. N. Brown, R. E. Kass, and P. P. Mitra, "Multiple neural spike train data analysis: state-of-the-art and future challenges," *Nature Neurosci.*, vol. 7, pp. 456–461, 2004.
[66] A. M. Chan, F. T. Sun, E. H. Boto, and B. M. Wingeier, "Automated seizure onset detection for accurate onset time determination in intracranial EEG," *Clin. Neurophysiol.*, vol. 119, no. 12, pp. 2687–2696, 2008.
[67] J. W. Pillow, Y. Ahmadian, and L. Paninski, "Model-based decoding, information estimation, and change-point detection techniques for multineuron spike trains," *Neural Comput.*, vol. 23, no. 1, pp. 1–45, 2011.

[68] C. Papadelis, Z. Chen, C. Kourtidou-Papadeli, P. D. Bamidis, I. Chouvarda, E. Bekiaris, and N. Maglaveras, "Monitoring sleepiness with on-board electrophysiological recordings for preventing sleep-deprived traffic accidents," *Clin. Neurophysiol.*, vol. 118, no. 9, pp. 1906–1922, 2007.
[69] Z. Chen and J. Wang, "Statistical analysis of neuronal population codes for encoding acute pain," in *Proc. IEEE Int. Conf. Acoustics Speech & Signal Processing*, 2016, pp. 829–833.
[70] N. G. Hatsopoulos and J. P. Donoghue, "The science of neural interface systems," *Annu. Rev. Neurosci.*, vol. 32, pp. 249–266, 2009.
[71] M. Y. Liberman, S. Ching, J. Chemali, and E. N. Brown, "A closed-loop anesthetic delivery system for real-time control of burst suppression," *J. Neural Eng.*, vol. 10, no. 4, pp. 046004, 2013.
[72] P. J. Grahn, G. W. Mallory, O. U. Khurram, B. M. Berry, J. T. Hachmann, A. J. Bieber, K. E. Bennet, P. H. Min, S. Chang, K. H. Lee, and J. L. Lujan, "A neurochemical closed-loop controller for deep brain stimulation: toward individualized smart neuromodulation therapies," *Front. Neurosci.*, vol. 8, no. 169, 2014.
[73] R. Pashaie, R. Baumgartner, T. J. Richner, S. K. Brodnick, M. Azimipour, E. K. W, and J. C. Williams, "Closed-loop optogenetic brain interface," *IEEE Trans. Biomed. Eng.*, vol. 62, no. 10, pp. 2327–2337, 2015.
[74] G. Dornhedge, J. del R. Millan, T. Hinterberger, D. J. McFarland, and K.-R. Müller, Eds., *Toward Brain-Computer Interfacing.* Cambridge, MA: MIT Press, 2007.
[75] M. A. L. Nicolelis and M. A. Lebedev, "Principles of neural ensemble physiology underlying the operation of brain-machine interfaces," *Nature Rev. Neurosci.*, vol. 10, pp. 530–540, 2009.
[76] G. Pfurtscheller and C. Neuper, "Motor imagery and direct brain-computer interface," *Proc. IEEE*, vol. 89, pp. 1123–1134, 2001.
[77] G. Pfurtscheller, C. Brunner, A. Schlögla, and F. H. L. da Silva, "Mu rhythm (de)synchronization and EEG single-trial classification of different motor imagery tasks," *NeuroImage*, vol. 31, no. 1, pp. 153–159, 2006.
[78] D. McFarland, L. Miner, T. M. Vaughan, and J. Wolpaw, "Mu and beta rhythm topographies during motor imagery and actual movements," *Brain Topogr.*, vol. 12, no. 3, pp. 177–186, 2000.
[79] S. Gao, Y. Wang, X. Gao, and B. Hong, "Visual and auditory brain-computer interfaces," *IEEE Trans. Biomed. Eng.*, vol. 61, no. 5, pp. 1436–1447, 2014.
[80] R. Fazel-Rezai, B. Z. Allison, S. E. W. Guger, C. S. C. Kleih, and A. Kübler, "P300 brain computer interface: current challenges and emerging trends," *Front. Neuroeng.*, vol. 5, pp. 14, 2012.
[81] B. Hong, F. Guo, T. Liu, X. Gao, and S. Gao "N200-speller using motion-onset visual response," *Nature*, vol. 120, no. 9, pp. 1658–1666, 2009.
[82] H. Ramoser, J. M. Gerking, and G. Pfurtscheller, "Optimal spatial filtering of single trial EEG during imagined hand movement," *IEEE Trans. Rehabil. Eng.*, vol. 8, no. 4, pp. 441–446, 2000.
[83] S. Lemm, B. Blankertz, G. Curio, and K. R. Muller, "Spatio-spectral filters for improving the classification of single trial EEG," *IEEE Trans. Biomed. Eng.*, vol. 52, no. 9, pp. 1541–1548, 2005.
[84] W. Wu, Z. Chen, S. Gao, and E. N. Brown, "A hierarchical Bayesian approach for learning sparse spatio-temporal decompositions of multichannel EEG," *NeuroImage*, vol. 56, no. 4, pp. 1929–1945, 2011.
[85] W. Wu, Z. Chen, X. Gao, Y. Li, E. Brown, and S. Gao, "Probabilistic common spatial patterns for multichannel EEG analysis," *IEEE Trans. Pattern Anal. Mach. Intell.*, vol. 37, no. 3, pp. 639–653, 2015.
[86] C. Lamus, M. S. Hamalainen, S. Temereanca, C. J. Long, E. N. Brown, and P. L. Purdon, "A spatiotemporal dynamic distributed solution to the MEG inverse problem," *NeuroImage*, vol. 63, no. 2, pp. 894–909, 2012.
[87] W. Penny, Z. Ghahramani, and K. Friston, "Bilinear dynamical systems," *Phil. Trans. R. Soc. Lond. B Biol. Sci.*, vol. 360, pp. 983–993, 2005.
[88] J. Vogelstein, B. Watson, A. Packer, R. Yuste, B. Jedynak, and L. Paninski, "Spike inference from calcium imaging using sequential Monte Carlo methods," *Biophys. J.*, vol. 97, no. 2, pp. 635–655, 2009.
[89] J. Vogelstein, A. Packer, T. A. Machado, T. Sippy, B. Babadi, R. Yuste, and L. Paninski, "Fast nonnegative deconvolution for spike train inference from population calcium imaging," *J. Neurophysiol.*, vol. 104, pp. 3691–3704, 2010.
[90] J. Onativia, S. R. Schultz, and P. L. Dragotti, "A finite rate of innovation algorithm for fast and accurate spike detection from two-photon calcium imaging," *J. Neural Eng.*, vol. 10, p. 046017, 2013.
[91] E. A. Pnevmatikakis, D. Soudry, Y. Gao, T. A. Machado, et al., "Simultaneous denoising, deconvolution, and demixing of calcium imaging data," *Neuron*, vol. 89, no. 2, pp. 285–299, 2016.
[92] J. Sui, T. Adali, Q. Yu, and V. D. Calhoun, "A review of multivariate methods for multimodal fusion of brain imaging data," *J. Neurosci. Methods*, vol. 204, no. 1, pp. 68–81, 2012.
[93] K. Uludag and A. Roebroeck, "General overview on the merits of multimodal neuroimaging data fusion," *NeuroImage*, vol. 102, pp. 3–10, 2014.
[94] J. Wang, F. Wagner, D. A. Borton, et al., "Integrated device for combined optical neuromodulation and electrical recording for chronic in vivo applications," *J. Neural Eng.*, vol. 9, pp. 016001, 2012.
[95] M. M. Shanechi, J. J. Chemali, M. Liberman, K. Solt, and E. N. Brown, "A brain-machine interface for control of medically-induced coma," *PLoS Comput. Biol.*, vol. 9, no. 10, pp. e1003284, 2013.
[96] A. Oswal, A. Jha, S. Neal, et al., "Analysis of simultaneous meg and intracranial lfp recordings during deep brain stimulation: A protocol and experimental validation," *J. Neurosci. Methods*, vol. 261, pp. 29–46, 2016.
[97] K. Edakawa, T. Yanagisawa, H. Kishima, R. Fukuma, S. Oshino, H. M. Khoo, M. Kobayashi, M. Tanaka, and T. Yoshimine, "Detection of epileptic seizures using phase-amplitude coupling in intracranial electroencephalography," *Sci. Rep.*, vol. 6, pp. 25422, 2016.
[98] T. N. Alotaiby, S. A. Alshebeili, T. Alshawi, I. Ahmad, and F. E. A. El-Sami, "EEG seizure detection and prediction algorithms: A survey," *EURASIP J. Adv. Signal Process.*, vol. 2014, pp. 183, 2014.
[99] N. Ahammad, T. Fathima, and P. Joseph, "Detection of epileptic seizure event and onset using EEG," *BioMed. Res. Int.*, vol. 2014, pp. 450573, 2014.
[100] J. P. Cunningham and B. M. Yu, "Dimensionality reduction for large-scale neural recordings," *Nature Neurosci.*, vol. 17, no. 11, pp. 1500–1509, 2014.
[101] Z. Chen, S. N. Gomperts, J. Yamamoto, and M. A. Wilson, "Neural representation of spatial topology in the rodent hippocampus," *Neural Comput.*, vol. 26, no. 1, pp. 1–39, 2014.
[102] B. M. Yu, J. P. Cunningham, G. Santhanam, S. I. Ryu, K. V. Shenoy, and M. Sahani, "Gaussian-process factor analysis for low-dimensional single-trial analysis of neural population activity," *J. Neurophysiol.*, vol. 102, no. 1, pp. 614–635, 2009.
[103] Y. Li, Z. Yu, N. Bi, Y. Xu, Z. Gu, and S. I. Amari, "Sparse representation for brain signal processing: A tutorial on methods and applications," *IEEE Signal Process. Mag.*, vol. 31, no. 3, pp. 96–106, 2014.
[104] D. Ba, B. Babadi, P. L. Purdon, and E. N. Brown, "Robust spectrotemporal decomposition by iteratively reweighed least squares," *Proc. Natl. Acad. Sci. U.S.A.*, vol. 111, no. 50, pp. E5336–E5345, 2014.
[105] B. Babadi, G. Obregon-Henao, C. Lamus, M. S. Hämäläinen, E. N. Brown, and P. L. Purdon, "A subspace pursuit-based iterative greedy hierarchical solution to the neuromagnetic inverse problem," *NeuroImage*, vol. 87, pp. 427–443, 2014.
[106] K. G, and W. S. G, *Bayesian Nonparametric Modeling and Data Analysis*. Boca Raton, FL: CRC, 2016.
[107] D. Jäckel, U. Frey, M. Fiscella, F. Franke, and A. Hierlemann, "Applicability of independent component analysis on high-density microelectrode array recordings," *J. Neurophysiol.*, vol. 108, no. 1, pp. 334–348, 2012.
[108] J. Dragas, D. Jäckel, A. Hierlemann, and F. Franke, "Complexity optimisation and high-throughput low-latency hardware implementation of a multi-electrode spike-sorting algorithm," *IEEE Trans. Neural Syst. Rehabil. Eng.*, vol. 23, no. 2, pp. 149–158, 2015.
[109] K. Balasubramanian, "Reconfigurable embedded system architecture for next-generation neural signal processing," in *Proc. IEEE Engineering Medicine and Biology Conf.*, 2010, pp. 1691–1694.
[110] D. Wang, Y. Hao, X. Zhu, T. Zhao, Y. Wang, Y. Chen, W. Chen, and X. Zheng, "FPGA implementation of hardware processing modules as coprocessors in brain-machine interfaces," in *Proc. IEEE Engineering Medicine and Biology Conf.*, 2011, pp. 4613–4616.
[111] S. Gibson, J. W. Judy, and D. Markovic, "An FPGA-based platform for accelerated offline spike sorting," *J. Neurosci. Methods*, vol. 215, no. 1, 2013.
[112] D. Fan, D. Rich, T. Holtzman, P. Ruther, J. W. Dalley, A. Lopez, et al., "A wireless multi-channel recording system for freely behaving mice and rats," *PLoS One*, vol. 6, no. 7, pp. e22033, 2011.
[113] G. N. Angotzi, F. Boi, S. Zordan, A. Bonfanti, and A. Vato, "A programmable closed-loop recording and stimulating wireless system for behaving small laboratory animals," *Sci. Rep.*, vol. 4, pp. 5963, 2014.
[114] T. Hasegawa, H. Fujimoto, K. Tashiro, M. Nonomura, A. Tsuchiya, and D. Watanabe, "A wireless neural recording system with a precision motorized microdrive for freely behaving animals," *Sci. Rep.*, vol. 5, pp. 7853, 2015.